streptomycin. Primary chondrocytes were harvested from 2-day-old mice with a C57BL/6J background. Briefly, articular cartilage of the femoral heads, femoral condyles, and tibial plateaus was isolated from mice and digested by 3 mg/ml collagenase D (Roche Applied Science) for 45 min, followed by 0.5 mg/ml collagenase D overnight. The chondrocytes were filtered through a sterile 40-μm cell strainer and cultured in DMEM/Ham's F-12 (1:1) containing 10% FBS, 100 units/ml penicillin G, and 100 μg/ml streptomycin. Differentiation of the cells, cultured in monolayer, was induced by the addition of recombinant human BMP-2 (PeproTech) at a concentration of 300 ng/ml, with or without insulin/transferrin/selenium (ITS) supplement (Sigma) on collagen type I-coated culture plates (Iwaki).

Embryonic Bone Organ Culture—Metatarsal bone rudiments were harvested from C57BL/6J mouse embryos at 16.5 days post-coitum (E16.5) and cultured in DMEM/Ham's F-12 (1:1) supplemented with 10% FBS, and 100 units/ml penicillin G, and 100 μg/ml streptomycin, as described (42). Cultured bones were stained with Alcian blue and alizarin red dyes according to a standard protocol for skeletal preparation. Briefly, bones fixed in 96% ethanol were stained with 0.015% Alcian blue 8GX (Sigma) in a mixture solution of 96% ethanol/acetic acid (4:1) for 1 day, followed by a dehydration step in 100% ethanol. Dehydrated bones were immersed briefly in 1% potassium hydroxide (KOH), followed by staining in 0.001% alizarin red S (Sigma) in 1% KOH for 1 day. Images were captured with stereomicroscope M165FC (Leica). Four bones per group were analyzed. Animal experiments were approved by the Institutional Animal Care and Use Committee of Kagoshima University (number MD12043).

RNA Interference—Dharmacon siRNA ON-TARGETplus SMARTpool, a mixture of four independent siRNAs against mouse *Runx1*, *Runx2*, *Runx3*, *Smpd3*, or *Has2*, and the control reagent were purchased from Thermo Scientific. siRNAs were transfected into cells using Lipofectamine RNAiMax (Invitrogen). BMP-2 and compounds were added to the culture simultaneously after an overnight transfection of siRNA.

Plasmids and Adenovirus—Mouse *Smpd3* cDNA was cloned from ATDC5 by employing an RT-PCR-based technique, subcloned into the entry vector, pENTR, and further transferred into the C-terminally V5-tagged expression vector, pEF-DEST51, by attL-attR recombination (Invitrogen). To generate adenovirus-carrying *Smpd3* cDNA, the *Smpd3* gene in the pENTR-Smpd3 vector was transferred into the C-terminally V5-tagged adenovirus expression vector pAd/CMV/V5-DEST by attL-attR recombination (Invitrogen) and further transfected into the adenovirus-producing cell line 293A according to the manufacturer's protocol. pAd/CMV/V5-GW/lacZ adenovirus expression vector was used as a control to express β-galactosidase. Adenovirus infection into ATDC5 cells was performed at a multiplicity of infection of 10. These experiments were approved by the Kagoshima University safety control committee for gene recombination techniques (number 22053).

Chemical Inhibitor Compounds and C_2-ceramide—All of the following agents were resolved in dimethyl sulfoxide (DMSO), and DMSO was used as the mock control. Cycloheximide was purchased from Sigma and applied at a concentration of 10 mM for 2 h, prior to BMP-2 stimulation. The nSMase inhibitor, GW4869 (Sigma), or C_2-ceramide (Enzo Life Sciences) was applied at the same time of BMP-2 induction, at 1 or 10 μM, respectively. The PI3K inhibitor, LY294002 (Sigma), Akt inhibitor, MK2206 (Chemie Tek), and the mammalian target of rapamycin inhibitor (Sigma) were applied at the same time of BMP-2 induction, at the indicated concentrations.

Immunoblotting and RTK Signaling Antibody Array Analysis—Cells were lysed in M-PER lysis buffer (Thermo Scientific) supplemented with aprotinin, sodium orthovanadate, and phenylmethylsulfonyl fluoride (PMSF) and subjected to SDS-PAGE, membrane transfer, and chemiluminescence, using standard protocol. Blots were incubated with the following: anti-Runx2 (1:1,000, 8G5, MBL); anti-nSMase2 (1:500, H-195, Santa Cruz Biotechnology); anti-aggrecan (1:500, H-300, Santa Cruz Biotechnology); anti-collagen type II α1 (1:1,000, LSBio); anti-phospho-Akt (Ser-473) (1:1,000, 587F11, Cell Signaling); anti-Akt (1:1,000, 5G3, Cell Signaling); anti-phospho-S6 ribosomal protein (Ser-235/236) (1:1,000, D57.2.2E, Cell Signaling); anti-S6 ribosomal protein (1:1,000, 54D2, Cell Signaling); anti-phospho-PI3K (1:1,000, number 4228, Cell Signaling); anti-PI3K (p85) (1:1,000, number 610045, BD Transduction Laboratories); anti-phospho-Smad1/5/8 (1:1,000, number 9511, Cell Signaling); anti-Smad1 (1:1,000, number 9743, Cell Signaling); and horseradish peroxidase (HRP)-conjugated anti-rabbit secondary antibody, anti-mouse secondary antibody (1:10,000) (Cell Signaling), or anti-tubulin antibody (1:1,000, DM1A, T9026, Sigma). Signals were detected using the LAS 4000 Mini Image Analyzer (Fujifilm). We employed PathScan® RTK signaling antibody array kit (Cell Signaling) to analyze the signaling pathway influenced by loss of Smpd3/nSMase2 function. This system is a slide-based antibody array, founded upon the sandwich immunoassay principle and allowing for the simultaneous detection of 28 receptor tyrosine kinases and 11 important signaling nodes when phosphorylated at tyrosine or other residues, was employed to analyze the signaling pathway influenced by loss of *Smpd3*/nSMase2 function. The experiment was performed according to the manufacturer's manual, and the chemiluminescent readout was performed with LAS 4000 Mini Image Analyzer.

Immunocytochemistry and Immunohistochemistry—For immunocytochemistry, cells were fixed with 4% paraformaldehyde in PBS for 30 min and treated with 0.2% Triton X-100. CAS block (Zymed Laboratories Inc.) was used for blocking. For immunohistochemistry, formalin-fixed mouse E17.5 embryo humeri were embedded in paraffin blocks, which were sliced at a 4-μm thickness. The antigen was retrieved by the Liberate Antibody Binding solution (Polysciences). A CAS block was used for blocking. Cells or bone sections were incubated with anti-aggrecan (1:100, H-300, Santa Cruz Biotechnology), anti-collagen type II α1 (1:100, LSBio), anti-nSMase2 rabbit polyclonal antibody (1:100, H-195, Santa Cruz Biotechnology), and anti-Has2 mouse monoclonal antibody (1:100, D-8, Santa Cruz Biotechnology). Anti-mouse Alexa Fluor 488 (1:200, A11001) or anti-rabbit Alexa Fluor 568 (1:200, A11011) (Invitrogen) was used to detect signals. Normal rabbit or mouse IgG was used as negative control. Hyaluronan (HA) detection

involved the following protocol. Samples were blocked with a streptavidin/biotin blocking kit (Vector Laboratories), according to the manufacturer's protocol, and digested sequentially with 0.05% of trypsin and 1 unit/ml of chondroitinase ABC (Sigma). Samples were further blocked with CAS block and sequentially incubated with biotin-conjugated HA-binding protein (1:1,000, Hokudo) and 1 μg/ml Alexa Fluor 488-conjugated streptavidin (Invitrogen). Images of immunocytochemistry and immunohistochemistry were captured with microscope AX80 and digital camera DP70 (Olympus). Animal experiments were approved by the Institutional Animal Care and Use Committee of Kagoshima University (number MD12043).

Real Time Quantitative PCR Assay—Cells were lysed with the TRIzol reagent (Invitrogen) to purify RNA, and 1 μg of RNA was reverse-transcribed into cDNA using the Verso cDNA kit (Thermo Scientific). The relative amount of gene transcripts was determined by real time PCR using the SYBR premix Ex TaqII (Takara) and the Thermal Cycler Dice TP850 (Takara). PCRs were performed in duplicate per sample, and the measured expression level of each gene was normalized to that of *Hprt1*. ΔC_t values were calculated by subtracting C_t values of *Hprt1* from C_t values of target genes. Sequence information of primers used is listed in supplemental Table 1.

TUNEL Assay—For detecting ATDC5 cells that underwent apoptosis, we used the ApopTag® peroxidase *in situ* apoptosis detection kit (Merck), which detects apoptotic cells *in situ* by labeling and detecting DNA strand breaks by the TUNEL method. The apoptotic cells were visualized by immunoperoxidase staining. Four independent experiments were performed, and four fields per well were evaluated for the number of apoptotic cells.

Statistical Analysis—Data in this study are expressed as mean ± S.D. of three independent experiments, unless otherwise noted. The statistical comparisons between the different treatments were performed using an unpaired Student's *t* test in which $p < 0.05$ was considered significant and $p < 0.01$ was highly significant.

RESULTS

Smpd3 Is Induced by BMP-2 in Chondrocytes and Is Detected in Mature Chondrocytes in Vivo—We hypothesized that BMP signaling cell-autonomously activated unknown mechanisms to terminate BMP-induced chondrocyte differentiation through a negative feedback pathway. We focused on the *Smpd3* gene, because it could be up-regulated by BMP-2 in C2C12 myoblasts of mesenchymal origin (39); loss-of-function models for *Smpd3* in mice showed an increased number of hypertrophic chondrocytes or retarded transition of proliferative chondrocytes into hypertrophic chondrocytes. Molecular mechanisms for both cartilage phenotypes are unclear (37, 38), suggesting a relationship between BMP signaling and *Smpd3*/nSMase2 in chondrogenesis. To investigate the possible cell-autonomous roles of *Smpd3* in chondrocyte maturation, we mainly employed the clonal chondrogenic mouse cell line ATDC5 because it is an excellent *in vitro* model for skeletal development, which can be stimulated by BMP-2 (43, 44). We also used the normal human chondrocyte cell line C28/I2, mouse chondrogenic cell line C3H10T1/2, and mouse primary articular chondrocytes. We used BMP-2 to stimulate chondrogenic differentiation because, in addition to existing evidence, we and others have observed strong expression of the BMP-2 protein in proliferating and mature chondrocytes in the developing bones of rodents (45, 46). We first checked if these cell lines could differentiate into chondrocytes and mature into hypertrophic chondrocytes and not fibrochondrocytes. Upon BMP-2 induction, ATDC5 cells could produce chondrocyte-specific proteins, aggrecan and type II collagen, in the extracellular matrix (Fig. 1*A*). The early chondrocyte differentiation marker aggrecan (*Acan*) was elevated after day 1 and was maintained at elevated levels for 2 weeks, whereas *Col10a1* increased mildly from day 3 and was strongly up-regulated after day 7. *Col1a1* and *Col3a1* gene expression was not elevated, but rather decreased, suggesting that these cells did not differentiated into fibrochondrocytes (Fig. 1*B*). Similar results were obtained in C28/I2 cells (Fig. 1, *C* and *D*) and C3H10T1/2 cells (Fig. 1*E*). We also confirmed chondrogenic differentiation of primary chondrocytes by BMP-2 (Fig. 1*F*). ΔC_t values of quantitative PCR data indicated that primary chondrocytes express higher levels of chondrocyte marker genes than the three chondrogenic cell lines, suggesting that primary chondrocytes are already committed and differentiated into chondrocytes without BMP-2 induction, whereas the cell lines are relatively immature to differentiate into chondrocytes upon BMP stimulation. From these expression profiles, we considered these cell lines to be suitable models for chondrocyte differentiation. In ATDC5 cells, *Smpd3* showed a varied expression pattern from that of *Acan* and *Col10a1*, in that it was strongly elevated from day 1 and showed a second peak of increase after day 7 (Fig. 1*G*). We also observed the BMP-2-induced increment of the *Smpd3* gene in C28/I2, C3H10T1/2, and primary chondrocytes (Fig. 1*H*). Importantly, the primary chondrocytes also expressed higher levels of *Smpd3*, suggesting its functional importance in chondrocytes. If *Smpd3*/nSMase2 has an *in vivo* role in chondrogenesis or cartilage maintenance, it would be expressed in cartilage, although its expression in cartilage has not been characterized in detail. Quantitative PCR analysis on a panel of cDNAs from multiple tissues generated from 3-month-old mice revealed that *Smpd3* was expressed at the highest levels in the thymus, intestine, skin, fat, and bone, although it was almost absent in the heart, liver, and kidney (Fig. 1*I*). *Smpd3* was moderately expressed in cartilage tissue. This expression profile of *Smpd3* is essentially similar to the results reported for 2-week-old mice (36). In embryonic bone, we detected prominent expression of *Smpd3*-coding nSMase2 protein in the bone collar and trabecular bone by immunofluorescence (Fig. 1*J*). In the cartilage, little nSMase2 expression was noted in resting and columnar proliferating chondrocytes, whereas relatively high expression was observed in the prehypertrophic layer and hypertrophic chondrocytes (Fig. 1*J*), with an expression pattern resembling that of Runx2 (4).

BMP-2-induced Increase of Smpd3 Expression Is Runx2-dependent—We wondered if this BMP-2-induced expression of *Smpd3* in ATDC5 was directed by the BMP-Smad signaling axis, although the expression pattern was not the typical rapid pattern of a gene that is directly targeted (47). To test this, we treated ATDC5 cells with cycloheximide (CHX), an inhibitor of

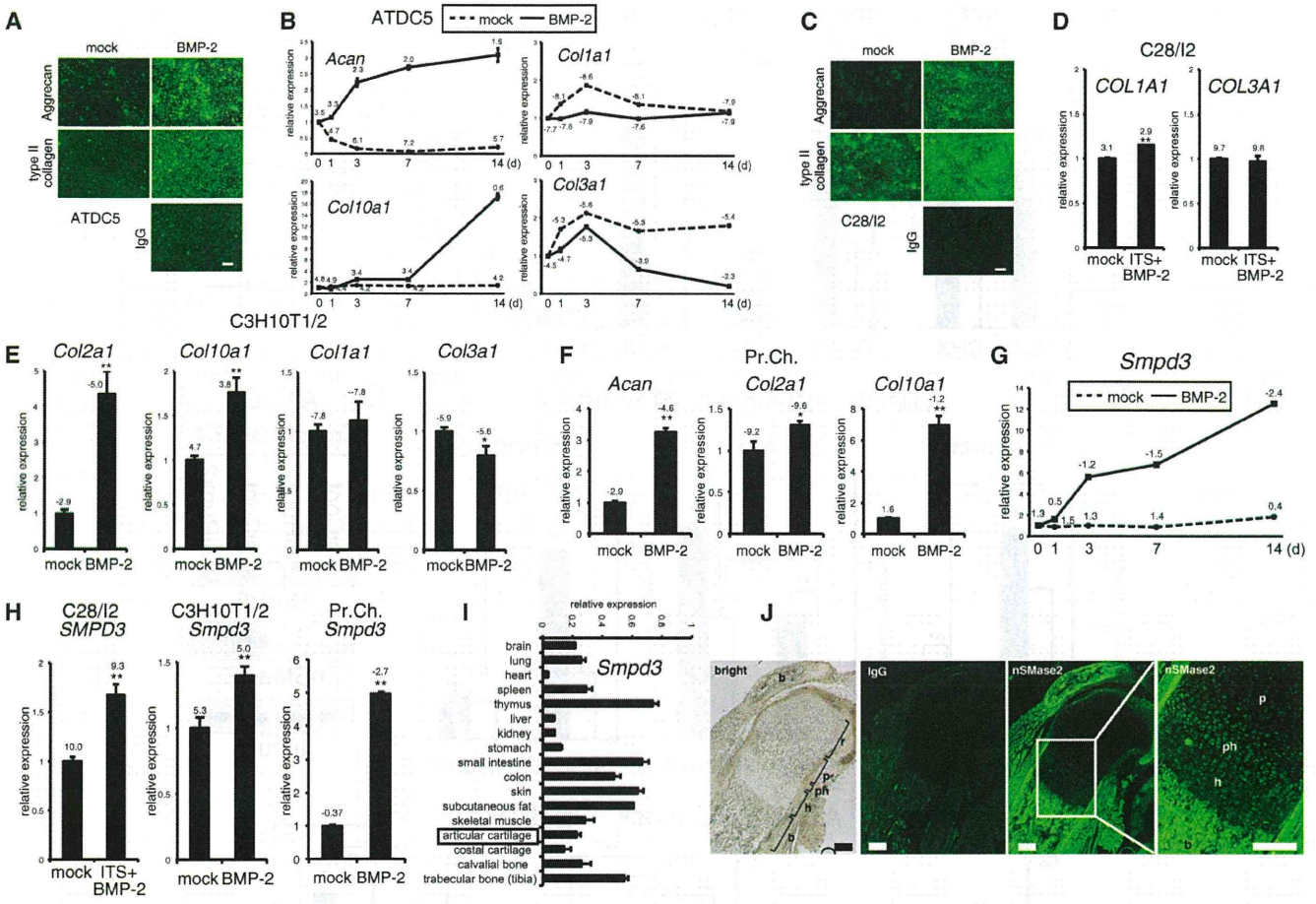

FIGURE 1. **Expression of *Smpd3*/nSMase2 is promoted by BMP-2 treatment in maturing chondrocytes *in vitro* and is increased in prehypertrophic and hypertrophic chondrocytes in a growth plate *in vivo*.** *A*, chondrogenic differentiation of mouse ATDC5 chondrocytes was induced by application of BMP-2 (300 ng/ml) for 7 days (*d*). Immunofluorescence for aggrecan or type II collagen was performed, with normal IgG as negative control. *Scale bar*, 100 μm. *B*, ATDC5 cells were cultured in the presence of BMP-2 (300 ng/ml) for the indicated periods. Expression levels of *Acan*, *Col10a1*, *Col1a1*, and *Col3a1* were examined by quantitative RT-PCR. *C*, chondrogenic differentiation of human C28/I2 chondrocytes was induced by the application of BMP-2 (300 ng/ml) for 7 days. Immunocytochemistry for aggrecan or type II collagen was performed, with normal IgG as negative control. *Scale bar*, 100 μm. *D*, C28/I2 chondrocytes were cultured in presence of BMP-2 (300 ng/ml) and ITS supplement for 14 days. Expression of *COL1A1* or *COL3A1* was evaluated by quantitative RT-PCR. *E*, mouse C3H10T1/2 cells were cultured with BMP-2 (300 ng/ml) for 48 h. Expression levels of *Col2a1*, *Col10a1*, *Col1a1*, and *Col3a1* were evaluated by quantitative RT-PCR. *F*, mouse primary chondrocytes (*Pr.Ch.*) cells were cultured in the presence of BMP-2 (300 ng/ml) for 6 days. Expression levels of *Acan*, *Col2a1*, and *Col10a1* were evaluated by quantitative RT-PCR. *G*, ATDC5 cells were cultured in presence of BMP-2 (300 ng/ml) for the indicated periods. Expression of *Smpd3* was examined by quantitative RT-PCR. *H*, quantitative RT-PCR for *Smpd3* was performed on samples in *D*, *E*, and *F*. *I*, real time PCR for *Smpd3* was performed on a tissue cDNA panel of a 3-month-old mouse. *J*, expression of nSMase2 in mouse E17.5 humerus cartilage was evaluated by immunofluorescence. Normal IgG was used as negative control. *r*, resting chondrocytes; *p*, proliferating chondrocytes; *ph*, prehypertrophic chondrocytes; *h*, hypertrophic chondrocytes; *b*, bone. *Scale bar*, 200 μm. *, $p < 0.05$; **, $p < 0.01$. ΔC_t values (C_t target − C_t Hprt1) of quantitative RT-PCR are indicated in the *graphs*.

de novo protein synthesis, before adding BMP-2. As expected, 24 h after BMP-2 stimulation, the induction of *Id1*, a representative direct-target gene of the BMP-Smad pathway, was maintained, even in the presence of CHX (Fig. 2*A*). Induction of *Id1* was higher in CHX-treated cells, likely because of the suppression of inhibitory Smad6 synthesis (27). However, expression of *Col2a1* was eliminated by CHX treatment (Fig. 1*A*). This basal suppression by CHX probably results from an inhibition of the constitutive expression of Sox9 and downstream Sox5 and Sox6, transcription factors that cooperatively activate the promoter of *Col2a1* (2, 48). However, existing Sox proteins should be responsible for the partially increased expression of *Col2a1* by BMP-2. The basal expression level of *Smpd3* was also suppressed by CHX treatment. Unlike *Col2a1*, however, the CHX-eliminated basal expression of *Smpd3* was not up-regulated by BMP-2 (Fig. 2*A*) suggesting that a *de novo* protein other than the Sox trio was necessary for BMP-induced expression of *Smpd3* in ATDC5 cells. Because the Runx2 protein is a master regulator of chondrocyte maturation (4, 5), and its direct interaction with the *Smpd3* promoter is important for its expression in myoblasts (39), we investigated the relationship between Runx2 and expression of *Smpd3* in chondrocytes. We confirmed the increment of the *Runx2* gene during BMP-induced maturation of ATDC5 chondrocytes (Fig. 2*B*). To address this question, we transfected ATDC5 cells with *Runx2* siRNA. At day 2 of BMP-2 application, *Runx2* was weakly induced, and its expression was knocked down by the siRNA to about 40% that of the control (Fig. 2*C*). Expression of *Id1* was not decreased by siRunx2, but rather it was increased, suggesting that Runx2 is inhibitory of the BMP pathway during this early differentiation stage. Interestingly, loss of Runx2 not only suppressed basal expression of *Smpd3* but also completely blocked induction by

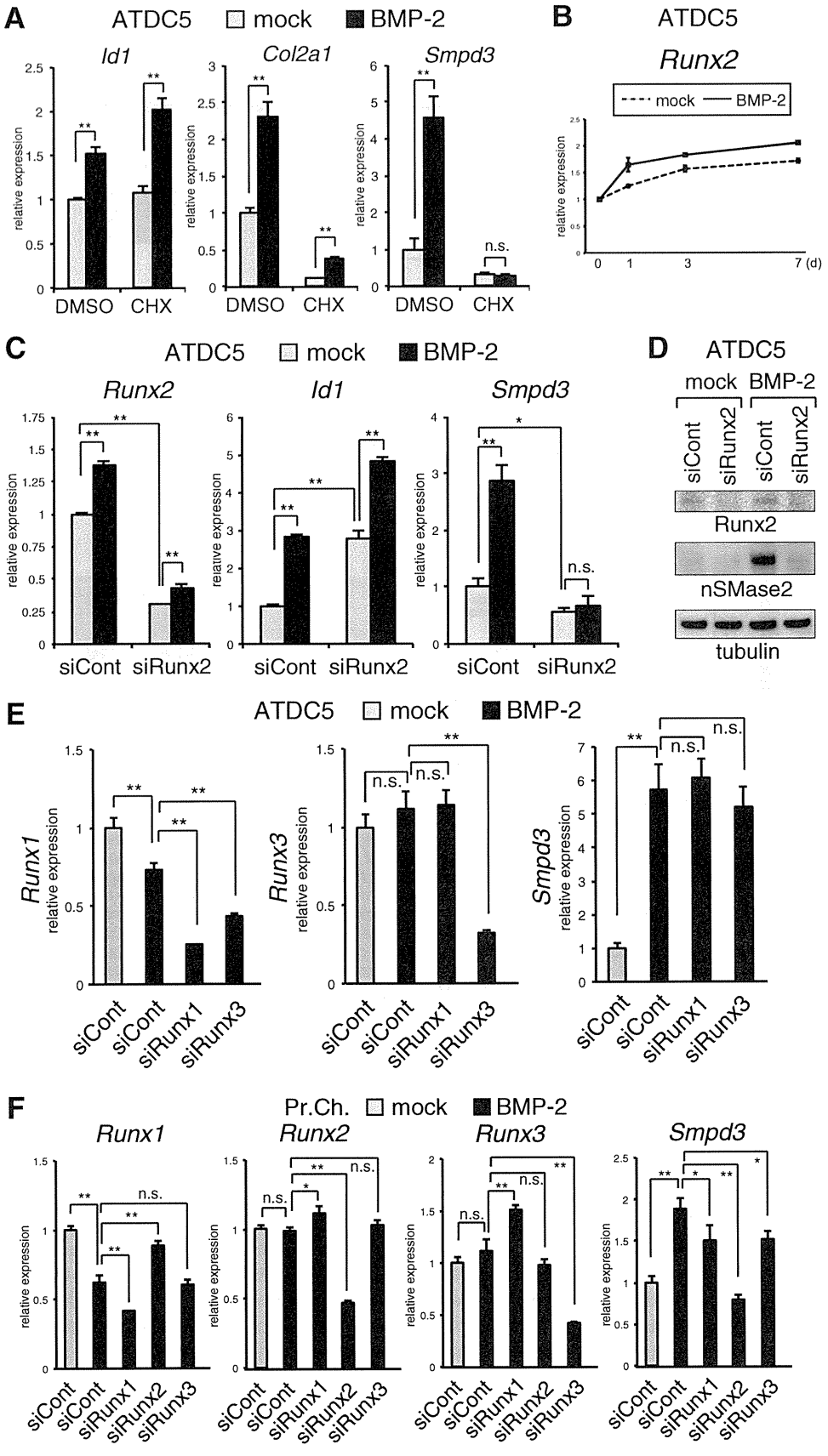
A
ATDC5
mock
BMP-2
Id1
Col2a1
Smpd3
relative expression
DMSO
CHX
n.s.
B
ATDC5
Runx2
mock
BMP-2
relative expression
0
1
3
7 (d)
C
ATDC5
mock
BMP-2
Runx2
Id1
Smpd3
relative expression
siCont
siRunx2
n.s.
D
ATDC5
mock
BMP-2
siCont
siRunx2
siCont
siRunx2
Runx2
nSMase2
tubulin
E
ATDC5
mock
BMP-2
Runx1
Runx3
Smpd3
relative expression
n.s.
siCont
siCont
siRunx1
siRunx3
F
Pr.Ch.
mock
BMP-2
Runx1
Runx2
Runx3
Smpd3
relative expression
n.s.
siCont
siCont
siRunx1
siRunx2
siRunx3

BMP-2 treatment (Fig. 2*C*). This effect of siRunx2 was confirmed by analyzing protein expression of nSMase2 using immunoblotting (Fig. 2*D*). To assess the functional specificity of Runx2 among the three Runx isoforms, siRNAs for *Runx1* and *Runx3* were tested in ATDC5 cells. Although we could obtain efficient knockdown of *Runx1* and *Runx3*, the BMP-2-induced increase of *Smpd3* was not blocked by the corresponding siRNA (Fig. 2*E*). In primary chondrocytes, knockdown of *Runx2* completely abrogated the BMP-stimulated up-regulation of *Smpd3* (Fig. 2*F*). In contrast to ATDC5 cells, silencing of *Runx1* or *Runx3* could mildly suppress expression of *Smpd3* in primary chondrocytes (Fig. 2*F*), suggesting that Runx1 and Runx3 were partially responsible for *Smpd3* expression. These data demonstrate that BMP signaling increases the expression of *Smpd3*/nSMase2 in chondrocytes in cooperation with Runx2, especially in the maturation stages when the level of *Runx2* is elevated.

Smpd3/nSMase2 and C_2-ceramide Inhibit Chondrogenic Differentiation and Maturation of Chondrocytes—We used a knockdown assay to investigate whether *Smpd3*/nSMase2 has a role in the differentiation of ATDC5 chondrocytes. The potent induction of *Smpd3* by BMP treatment was silenced by siSmpd3 at a level of ~25% of that in cells treated with control siRNA at day 6 (Fig. 3*A*). Loss of *Smpd3* mildly increased the basal level of *Col2a1* expression and significantly enhanced the BMP-2-induced increment (Fig. 3*A*). Although expression of *Col10a1* was not significantly elevated by BMP-2 at day 6, it was dramatically increased by siSmpd3 in the presence of BMP-2. Similar effects of siSmpd3 on the expression of *Col2a1* and *Col10a1* were observed in primary chondrocytes (Fig. 5*F*). This effect of *Smpd3* knockdown against expression of *Col2a1* was mimicked by the addition of 1 μM GW4869, a specific inhibitor compound for nSMase (Fig. 3*B*) (49), suggesting that the data from the siSmpd3 experiment resulted from down-regulation of nSMase2. GW4869 also enhanced the production of the cartilage-specific extracellular component, glycosaminoglycan, by BMP-2 stimulation for 17 days, as assessed by Alcian blue staining, both in ATDC5 cells and in primary chondrocytes (Fig. 3*C*). Because nSMase2 generates ceramide as a lipid second messenger from the cell membrane, and the total level of ceramide was decreased in *fro/fro* bone (36), we challenged the cell membrane-permeable C_2-ceramide to mimic nSMase-ceramide signaling. Combined application of GW4869 and C_2-ceramide completely eliminated the GW4869-mediated enhancement observed by Alcian blue staining (Fig. 3*C*). The effect of GW4869 or C_2-ceramide on Alcian blue staining was confirmed by immunoblotting for aggrecan (Fig. 3*C*). Although C_2-ceramide showed no effect on BMP-2-induced expression of *Smpd3* at day 14, it significantly suppressed the expression of both *Col2a1* and *Col10a1* (Fig. 3*D*). As another gain-of-function approach, adenovirus-mediated overexpression of *Smpd3* in ATDC5 cells was performed to yield transgene expression levels that were ~100 times those of endogenous levels even after 8 days of induction (Fig. 3*E*). Infection of *Smpd3*-expressing adenovirus presented similar results as those of the C_2-ceramide experiment, in which overexpression inhibited the BMP-2-mediated elevation of both *Col2a1* and *Col10a1* expression (Fig. 3*E*). Similarly, Smpd3-expressing adenovirus suppressed maturation of primary chondrocytes (Fig. 3*F*). These loss- or gain-of-function experiments suggest a cell-autonomous inhibitory action of the *Smpd3*/nSMase2-ceramide axis on maturation of chondrocytes.

Smpd3 Suppresses the Activity of the Akt-S6 Pathway during Chondrogenesis in Vitro—We sought the molecular mechanism by which Smpd3/nSMase2 suppresses chondrogenesis and focused on the Akt signaling pathway for the following reasons. First, phosphorylation of Akt and the downstream ribosomal protein S6 (rpS6) was increased in *fro/fro* fibroblasts (50). Second, genetic approaches revealed that the IGF-IGF receptor-PI3K-Akt pathway plays key roles in skeletal growth and endochondral ossification and that overexpression of the activated form of Akt in the cartilage of transgenic mice promoted chondrocyte differentiation and maturation, whereas forced expression of its dominant-negative form delayed these cellular events (51). To evaluate the specificity of Akt among the various RTK signaling pathways, we examined the possible correlation of the Akt pathway in *Smpd3*/nSMase2 signaling during chondrocyte differentiation by performing an RTK signaling antibody array assay. Because receptors for insulin or insulin-like growth factor (IGF), which promote chondrogenic differentiation of ATDC5 cells (40), are RTKs, and a mixture of ITS is preferentially used to prepare the chondrogenic condition of ATDC5 cells (52), we first checked the effect of application of the ITS supplement alone and found no effect on the RTK array (Fig. 4*A*). Interestingly, 8 h after the addition of BMP-2, phosphorylation of rpS6 was significantly strengthened. More importantly, BMP-2-enhanced rpS6 phosphorylation was further increased by GW4869 or *Smpd3* knockdown, and these loss-of-function conditions for *Smpd3*/nSMase2 induced mild phosphorylation of Akt (Fig. 4*A*), suggesting that Akt and rpS6 are the specific targets of inhibition. This notion was further supported by an immunoblot assay using ATDC5 cells treated with siSmpd3 or Smpd3-expressing adenovirus. Application of BMP-2, in combination with the ITS supplement, dramatically induced expression of the nSMase2 protein, which was clearly diminished by transfecting with siRNA for *Smpd3* (Fig. 4*B*), even after 20 h of stimulation. Phosphorylation of Akt, as well as of rpS6, was significantly increased by

FIGURE 2. **BMP-2-induced increase of *Smpd3* expression in chondrocytes is Runx2-dependent.** *A*, CHX was applied to ATDC5 cells at a concentration of 10 mM for 2 h prior to BMP-2 (300 ng/ml) stimulation. Cells were harvested 24 h after BMP-2 induction to perform quantitative RT-PCR analysis for *Id1*, *Col2a1*, and *Smpd3*. *B*, ATDC5 cells were cultured with BMP-2 (300 ng/ml) for the indicated times. Expression of *Runx2* was examined by quantitative RT-PCR. *C*, ATDC5 chondrocytes were transfected with control siRNA (*siCont*) or *Runx2* siRNA (*siRunx2*) for 16 h and then treated with or without BMP-2 (300 ng/ml) for 48 h. Quantitative RT-PCR analysis was performed for *Runx2*, *Id1*, and *Smpd3*. *D*, ATDC5 cells were transfected with control siRNA (*siCont*) or *Runx2* siRNA (*siRunx2*) for 16 h and stimulated with BMP-2 (300 ng/ml) for 48 h. Cells were subjected to immunoblot analysis for the indicated antibodies. Tubulin served as a loading control. *E*, ATDC5 cells were transfected with control siRNA (*siCont*), *Runx1* siRNA (*siRunx1*), or *Runx3* siRNA (*siRunx3*) for 16 h and then treated with or without BMP-2 (300 ng/ml) for 48 h. Quantitative RT-PCR analysis was performed for *Runx1*, *Runx3*, and *Smpd3*. *F*, mouse primary chondrocytes were transfected with control siRNA (*siCont*), *Runx1* siRNA (*siRunx1*), *Runx2* siRNA (*siRunx2*), or *Runx3* siRNA (*siRunx3*) for 16 h and then treated with or without BMP-2 (300 ng/ml) for 48 h. Quantitative RT-PCR analysis was performed for *Runx1*, *Runx2*, *Runx3*, and *Smpd3*. *, $p < 0.05$; **, $p < 0.01$; *n.s.*, not significant.

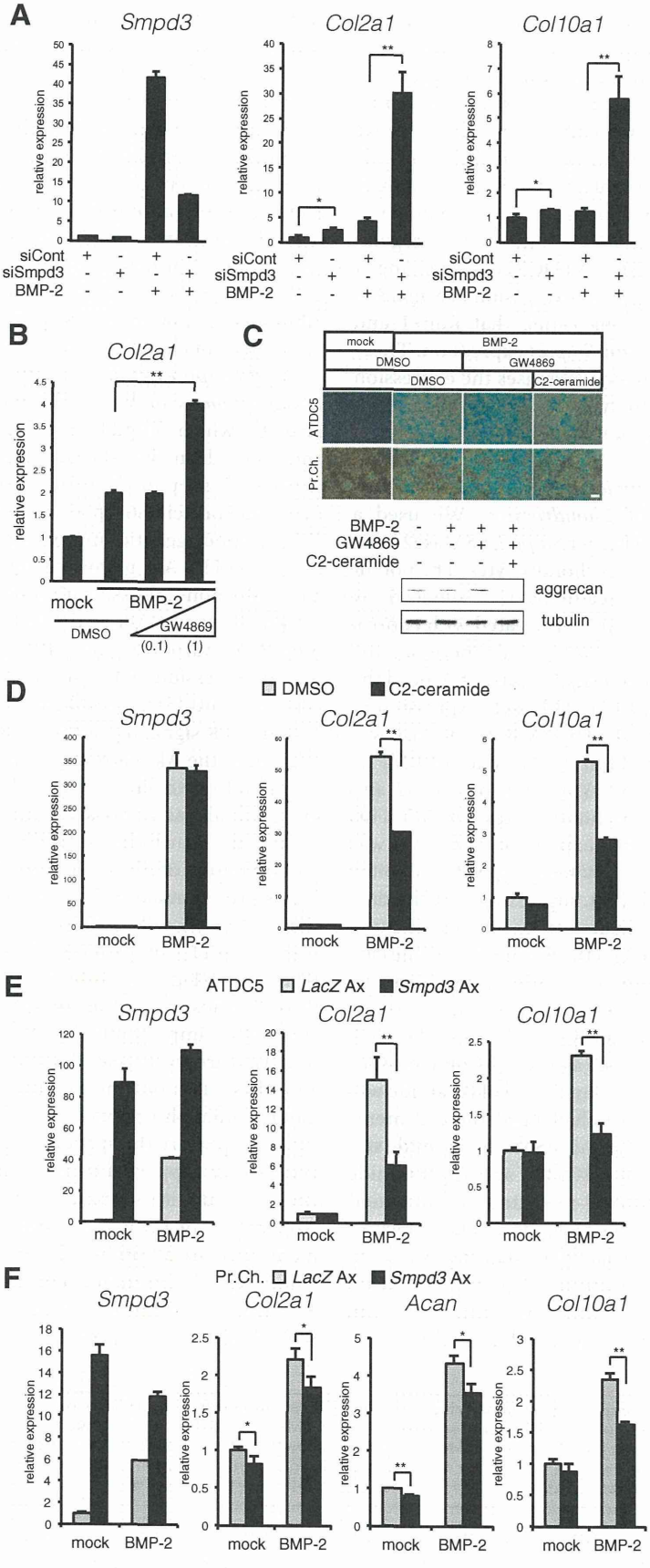
A
Smpd3
Col2a1
Col10a1
relative expression
siCont
siSmpd3
BMP-2
B
Col2a1
relative expression
mock
BMP-2
DMSO
GW4869
(0.1) (1)
C
mock
BMP-2
DMSO
GW4869
DMSO
C2-ceramide
ATDC5
Pr.Ch.
BMP-2
GW4869
C2-ceramide
aggrecan
tubulin
D
DMSO
C2-ceramide
Smpd3
Col2a1
Col10a1
relative expression
mock
BMP-2
E
ATDC5
LacZ Ax
Smpd3 Ax
Smpd3
Col2a1
Col10a1
relative expression
mock
BMP-2
F
Pr.Ch.
LacZ Ax
Smpd3 Ax
Smpd3
Col2a1
Acan
Col10a1
relative expression
mock
BMP-2

BMP-2 stimulation, although these proteins became more phosphorylated by the loss of *Smpd3* (Fig. 4*B*). Importantly, siSmpd3 increased the weak basal phosphorylation of both Akt and rpS6 in mock control cells, suggesting that neither ITS nor BMP-2 is crucial for the function of nSMase2. Overexpression of *Smpd3* weakened the induced phosphorylation of both Akt and rpS6 (Fig. 4*C*), whereas similar effects of Smpd3 adenovirus were observed in primary chondrocytes (Fig. 4*D*). Increased phosphorylation of Akt and rpS6 by the loss of *Smpd3* was also observed in primary chondrocytes (Fig. 4*D*) and C3H10T1/2 (Fig. 4*E*). The phosphorylation level of Smad1/5/8 was not altered by *Smpd3* knockdown (Fig. 4*E*), suggesting that the accelerated chondrogenic differentiation by siSmpd3 (Fig. 3*A*) was not due to an enhancement of BMP signaling. These results demonstrate an inhibitory function of *Smpd3*/nSMase2 against activation of Akt and rpS6 and a positive effect of BMP-2 in chondrocytes.

Smpd3 Suppresses Maturation of ATDC5 Chondrocytes via the PI3K-Akt Pathway—We next investigated the role of the Akt pathway in nSMase2-mediated inhibition of chondrogenesis in ATDC5 cells by employing specific inhibitor compounds. MK2206, an inhibitor for Akt, was tested for its ability to negate the enhanced chondrogenesis caused by loss of *Smpd3*. Expression of *Smpd3* in siSmpd3-treated cells was not further altered by MK2206 at concentrations between 1 and 3 μM, although 10 μM of the MK compound suppressed it (Fig. 5*A*). At day 6 of BMP-2 induction, MK2206 successfully suppressed the *Smpd3* siRNA-mediated increase of *Acan*, *Col2a1*, and *Col10a1*, in a dose-dependent fashion, at concentrations between 1 and 10 μM (Fig. 5*A*). Alcian blue staining revealed that the BMP-2-induced production of glycosaminoglycan, which was further stimulated by siSmpd3, was eliminated by the addition of MK2206 at 10 μM (Fig. 5*B*). We also investigated the participation of mammalian target of rapamycin, a downstream effector of Akt, by using its specific inhibitor, rapamycin. Although rapamycin suppressed the expression of *Smpd3*, it could block the siSmpd3-mediated up-regulation of *Col10a1* at 1 μM (Fig. 5*C*). Because total protein expression of PI3K, the upstream mediator of Akt, was significantly increased in *fro/fro* fibroblasts, which resulted in an up-regulated phosphorylation level of PI3K, we evaluated these in ATDC5 chondrocytes by an immunoblot assay. Indeed, phosphorylated, as well as total, PI3K protein was increased upon transfection with *Smpd3* siRNA (Fig. 5*D*). Therefore, a specific inhibitor for PI3K, LY294002, was tested with siSmpd3. LY294002 did not change the expression of *Smpd3* at concentrations between 1 and 5 μM, but a 25 μM concentration led to suppression. However, LY294002 did suppress the elevated expression of *Acan*, *Col2a1*, and *Col10a1* caused by the loss of *Smpd3*, in a dose-dependent manner at concentrations between 1 and 25 μM (Fig. 5*E*). The role of the Akt pathway was confirmed in primary chondrocytes by applying LY294002 (25 μM), MK2206 (5 μM), and rapamycin (0.5 μM); only MK2206 suppressed *Smpd3* expression (Fig. 5*F*). Hence, none of these inhibitor compounds increased expression of *Smpd3*, indicating that the inhibitory action on chondrocyte maturation was independent of *Smpd3* expression level. These data suggest that Smpd3/nSMase2 suppresses chondrocyte maturation, at least in part, via the PI3K-Akt pathway.

GW4869 or C_2-ceramide Promotes or Eliminates, Respectively, Terminal Hypertrophic Maturation of Chondrocytes in Mouse Bone Organ Culture—To further examine the role of the nSMase-ceramide signaling axis in relatively physiological conditions, we employed an *ex vivo* organ culture system of mouse embryonic metatarsal bone, a widely used method that permits the study of a complex chondrogenic process in a three-dimensional structure, in the context of native cell-cell and cell-extracellular matrix interactions and cellular signaling (42). The cartilage matrix was stained by Alcian blue, and the extracellular matrix calcified by mature hypertrophic chondrocytes was stained by alizarin red. The clear zone represents layers of uncalcified hypertrophic chondrocytes (Fig. 6*A*). All zone lengths were measured after image capturing (Fig. 6*B*). Blocking the function of nSMase by GW4869 solely enlarged both the clear zone and the calcified zone in a mild but statistically significant manner, a result similar to that seen by treatment with BMP-2 alone (Fig. 6, *A* and *B*, *2nd* and *3rd lanes*). Combined treatment with GW4869 and BMP-2 showed an additive effect (Fig. 6, *A* and *B*, *4th lane*), whereas C_2-ceramide eliminated the BMP-2-induced increase of the hypertrophic zone and, especially, the terminally differentiated calcified zone (Fig. 6, *A* and *B*, *5th lane*). Hence, GW4869 and C_2-ceramide exhibited opposite actions against BMP-2-driven acceleration in the hypertrophic conversion and terminal maturation of chondrocytes. In addition, C_2-ceramide clearly cancelled the additive promotion induced by GW4869 and BMP-2 (Fig. 6, *A* and *B*, *6th lane*). These results indirectly demonstrate the physiologically suppressive role of the nSMase2-ceramide pathway on chondrocyte maturation in cartilage/bone rudiments. Moreover, these data suggest a new strategy to control the rate of hypertrophic maturation in cartilage and bone regenerative medicine.

Apoptosis of terminally matured hypertrophic chondrocytes was reduced in the bone of *fro/fro* mice, a phenotype that accounted for the delayed onset of bone formation (36), suggesting an accelerating role for *Smpd3*/nSMase2 in the apoptosis of chondrocytes. To investigate whether this is a cell-autonomous event, we knocked down *Smpd3* in ATDC5 chondrocytes and performed a TUNEL assay to evaluate the

FIGURE 3. **Loss or gain of *Smpd3*/nSMase2 function promotes or suppresses BMP-2-induced chondrogenic maturation, respectively.** *A*, ATDC5 chondrocytes were transfected with control siRNA (*siCont*) or *Smpd3* siRNA (*siSmpd3*) for 16 h and then treated with or without BMP-2 (300 ng/ml) for 6 days. Quantitative RT-PCR analysis was performed for *Smpd3*, *Col2a1*, and *Col10a1*. *B*, ATDC5 cells were treated with BMP-2 (300 ng/ml) in combination with GW4869 at a concentration of 0.1 or 1 μM for 4 days to analyze expression of *Col2a1* by quantitative RT-PCR. *C*, ATDC5 cells or primary chondrocytes were stimulated with BMP-2 (300 ng/ml) in combination with GW4869 (1 μM) and C_2-ceramide (10 μM) for 17 days. Cells were subjected to Alcian blue staining. *Scale bar*, 200 μm. A parallel experiment was done with ATDC5 with a stimulation time of 7 days, and immunoblotting was performed for aggrecan and tubulin. *D*, ATDC5 cells were stimulated with BMP-2 (300 ng/ml) in combination with C_2-ceramide at 10 μM for 14 days. *E*, ATDC5 chondrocytes were infected with adenovirus (*Ax*) carrying *LacZ* or *Smpd3* for 2 h, and further cultured with or without BMP-2 (300 ng/ml) for 7 days. Expression of *Smpd3*, *Col2a1*, and *Col10a1* was evaluated by quantitative RT-PCR. *F*, mouse primary chondrocytes were infected with adenovirus carrying *lacZ* or *Smpd3* for 2 h and further cultured with or without BMP-2 (300 ng/ml) for 6 days. Expression of *Smpd3*, *Col2a1*, and *Col10a1* was evaluated by quantitative RT-PCR. *, $p < 0.05$; **, $p < 0.01$.

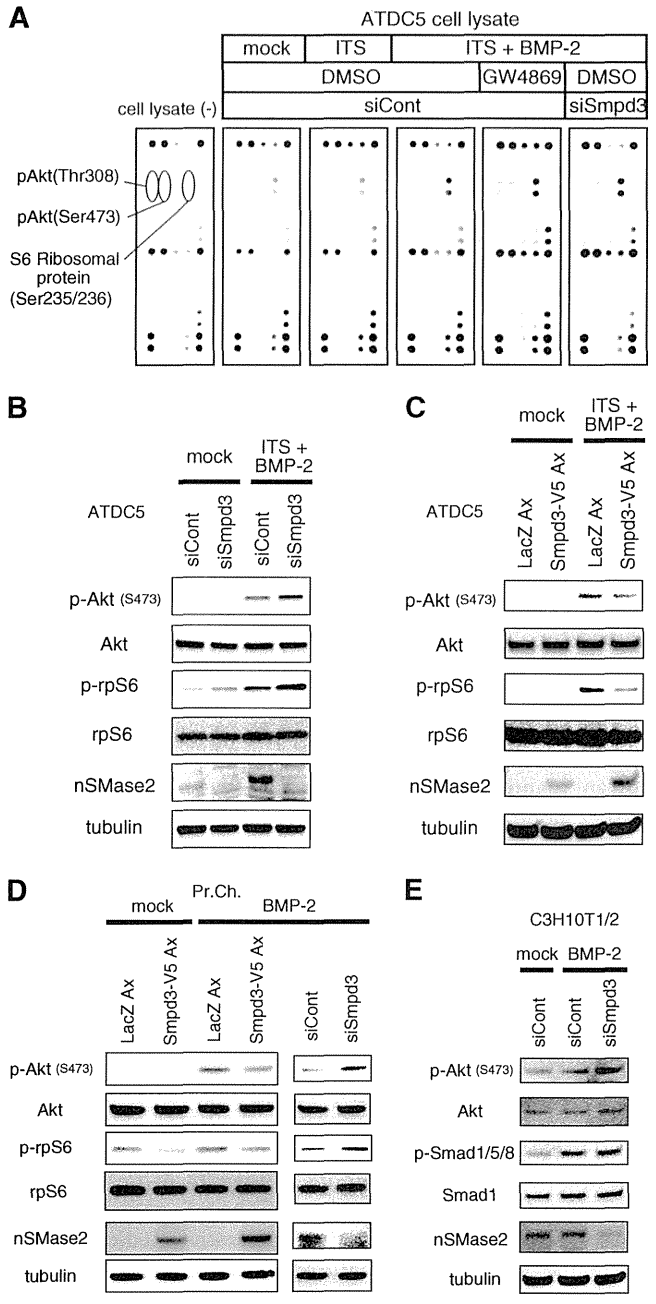

FIGURE 4. **Akt pathway is activated or repressed by loss or gain of *Smpd3* function, respectively.** *A*, ATDC5 cells were transfected with control siRNA (*siCont*) or *Smpd3* siRNA (*siSmpd3*) for 16 h, and then stimulated by a combination of ITS supplement and BMP-2 (300 ng/ml), with or without GW4869 (1 μM), for 8 h. Cells were analyzed by a PathScan® RTK signaling antibody array. *B* and *C*, ATDC5 cells were transfected with control siRNA (*siCont*) or *Smpd3* siRNA (*siSmpd3*) for 16 h (*B*) or infected with adenovirus (*Ax*) carrying *lacZ* or *Smpd3* for 2 h (C), and stimulated with the combination of ITS supplement and BMP-2 (300 ng/ml) for 20 h. Cells were subjected to immunoblot analysis for the indicated antibodies. Tubulin served as a loading control. *D*, mouse primary chondrocytes were infected with adenovirus carrying *lacZ* or *Smpd3* for 2 h or transfected with control siRNA (*siCont*) or *Smpd3* siRNA (*siSmpd3*) for 16 h and stimulated with BMP-2 (300 ng/ml) for 8 h. Cells were subjected to immunoblot analysis for the indicated antibodies. Tubulin served as a loading control. *E*, C3H10T1/2 cells were transfected with control siRNA (*siCont*) or *Smpd3* siRNA (siSmpd3) for 8 h and stimulated with BMP-2 (300 ng/ml) for 16 h. Cells were subjected to immunoblot analysis for the indicated antibodies. Tubulin served as a loading control.

effect on apoptosis (Fig. 6*C*). TUNEL-positive cells were counted after image capturing (Fig. 6*D*). Matured ATDC5 chondrocytes, stimulated by BMP-2 with ITS supplement for 6 days, showed hypertrophic morphology, and a substantial number of cells underwent apoptosis (Fig. 6, *C* and *D*). Indeed, transfection of *Smpd3* siRNA into maturing ATDC5 cells resulted in a statistically significant reduction in apoptosis (Fig. 6, *C* and *D*), suggesting that nSMase2 cell-autonomously accelerates apoptosis of hypertrophic chondrocytes.

Smpd3/nSMase2 Suppresses Expression of Has2 during Chondrogenesis via the PI3K-Akt Axis—Chondrocyte maturation is supported by hyaluronan, and embryonic limb mesoderm-specific ablation of hyaluronan synthase 2 (*Has2*) in mice resulted in reduced formation of zones for prehypertrophic and hypertrophic chondrocytes (53), suggesting a major role of Has2 in the three Has isoforms involved in the production of hyaluronan in cartilage. Recent studies have reported a significant level of *Has2* expression and hyaluronan synthesis in *fro/fro* fibroblasts and that nSMase2 suppressed production of Has2 via inactivation of Akt (50). Taken together, if *Smpd3*/nSMase2 also regulates expression of *Has2* in chondrocytes, Has2 might be another target for the inhibitory action of *Smpd3*/nSMase2 on chondrocyte hypertrophic maturation. We confirmed the crucial role of Has2 in chondrocyte differentiation and maturation; siRNA-mediated knockdown of *Has2* resulted in a decline in expression of *Col2a1* and *Col10a1*, both in ATDC5 cells (Fig. 7*A*) and primary chondrocytes (Fig. 7*B*). In ATDC5 chondrocytes, upon BMP-2 stimulation the expression of *Has2* was down-regulated by half at day 6, whereas silencing of *Smpd3* recovered the decline (Fig. 7*C*). Although expression of *Has1* and *Has3* was also suppressed by BMP-2 induction, *Smpd3* siRNA did not rescue the decrease (Fig. 7*C*), suggesting that only Has2, among the three Has isoforms, is a specific target of Smpd3 signaling in chondrocytes. This finding was confirmed using immunofluorescence for protein expression levels in ATDC5 cells (Fig. 7*D*) and primary chondrocytes (Fig. 7*E*), which indicated that although nSMase2 accumulated due to BMP-2 induction, the signals of Has2 protein were diminished. The merged images show the mutually exclusive expression of nSMase2 and Has2. Importantly, *Smpd3* knockdown rescued the weakened expression of Has2 protein (Fig. 7, *D* and *E*). The expression level of Has2 protein was reflected to the production of hyaluronan in primary chondrocytes (Fig. 7*E*). *In vivo*, both nSMase2 and Has2 were strongly expressed and co-localized in bone (Fig. 7*F*). In cartilage, however, Has2 was widely expressed in proliferating and resting chondrocytes with moderate strength, although it was diminished in the hypertrophic zone, where the expression pattern contrasted with that of nSMase2 being dominant in hypertrophic chondrocytes (Fig. 7*F*). Hyaluronan not only localized to the extracellular matrix of Has2-expressing chondrocytes in immature cartilage but also existed in the matrix of hypertrophic chondrocytes (Fig. 7*F*), suggesting that the low turnover rate may have caused its retention in the cartilage matrix, even after a decrease in Has2. Finally, we checked if the PI3K or Akt pathway was involved in the suppressive action of *Smpd3*/nSMase2 on *Has2*. The accelerated expression of *Has2* by silencing of *Smpd3* in the presence

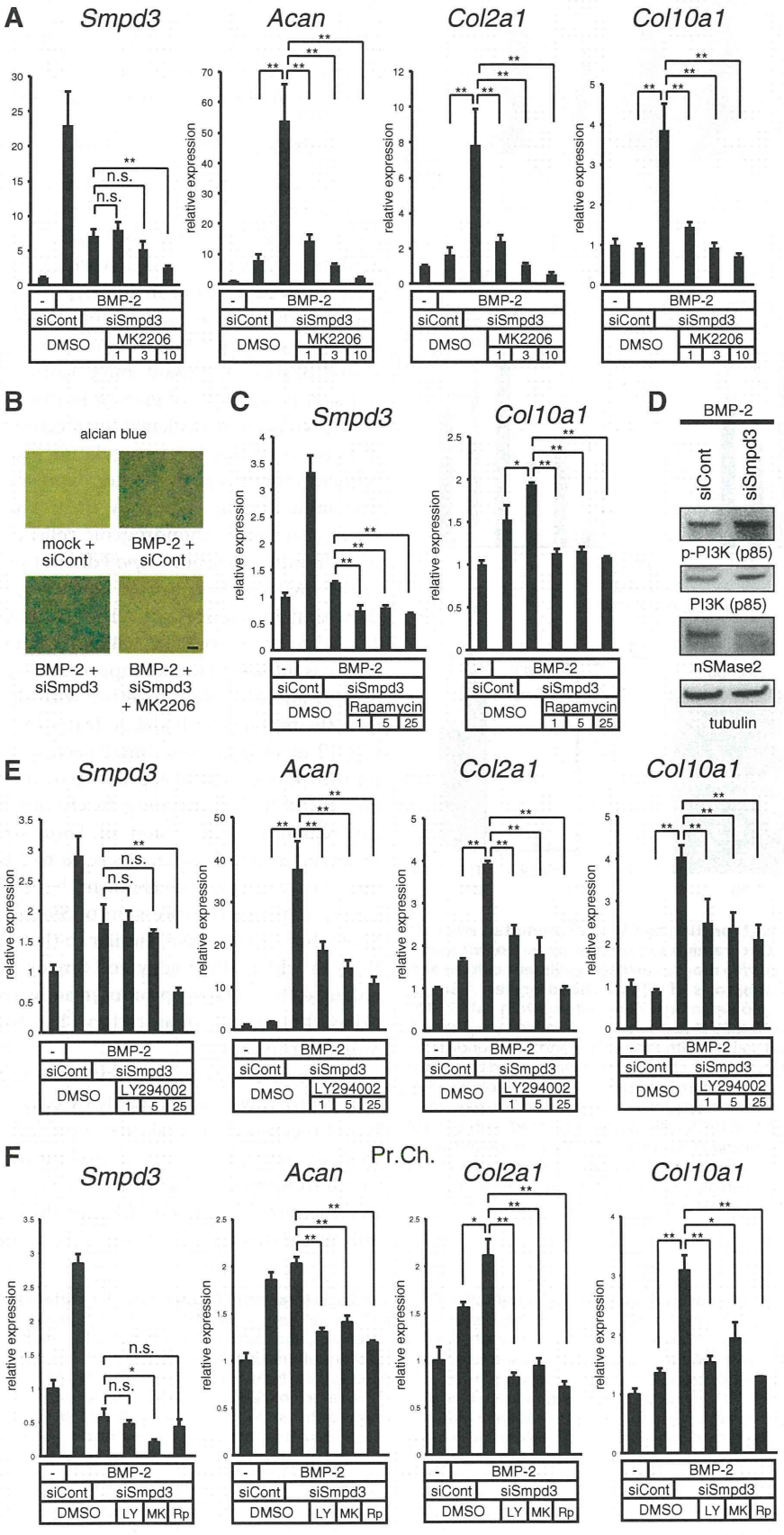
A
Smpd3
Acan
Col2a1
Col10a1
relative expression
n.s.
n.s.
-
BMP-2
siCont
siSmpd3
DMSO
MK2206
1
3
10
B
alcian blue
mock + siCont
BMP-2 + siCont
BMP-2 + siSmpd3
BMP-2 + siSmpd3 + MK2206
C
Smpd3
Col10a1
Rapamycin
1
5
25
D
BMP-2
siCont
siSmpd3
p-PI3K (p85)
PI3K (p85)
nSMase2
tubulin
E
Smpd3
Acan
Col2a1
Col10a1
LY294002
1
5
25
F
Pr.Ch.
Smpd3
Acan
Col2a1
Col10a1
LY
MK
Rp

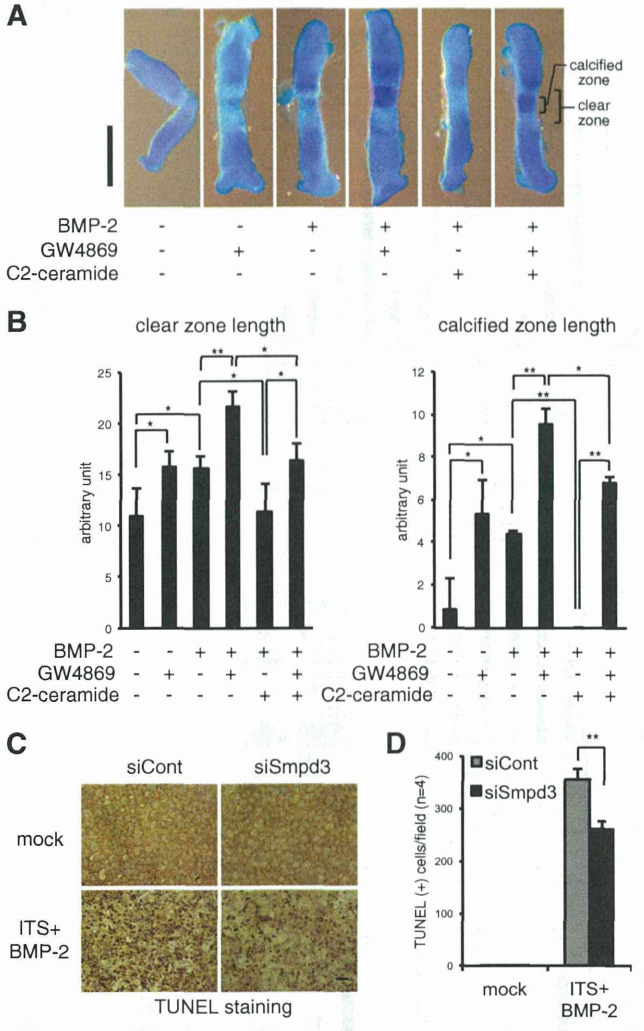

FIGURE 6. **Blocking of nSMase2 function by GW4869 promotes, whereas mimicking the function by C_2-ceramide suppresses, hypertrophic maturation of chondrocytes in *ex vivo* mouse cartilage rudiment culture and loss of *Smpd3* decreased apoptosis of ATDC5 chondrocytes.** *A* and *B*, metatarsal bones from E16.5 mouse embryo were cultured with BMP-2 (300 ng/ml) in combination with GW4869 (1 μM) and/or C_2-ceramide (10 μM) for 3 days. The cartilage matrix was stained with Alcian blue, and the chondrocyte matrix calcified by mature hypertrophic chondrocytes was stained by alizarin red (*A*). The *clear zone* represents hypertrophic chondrocytes. *Scale bar*, 500 μm. The length of the hypertrophic clear zone and the *calcified zone* were measured ($n = 4$) (*B*). *C* and *D*, ATDC5 cells were transfected with control siRNA (*siCont*) or *Smpd3* siRNA (*siSmpd3*) for 16 h and further stimulated by ITS supplement and BMP-2 (300 ng/ml) for 6 days. Apoptotic cells were visualized by TUNEL immunoperoxidase staining (*C*). *Scale bar*, 300 μm. The number of apoptotic cells was counted ($n = 4$) (*D*). *, $p < 0.05$; **, $p < 0.01$.

of BMP-2 treatment was negated by the addition of LY294002 or MK2206, suggesting that the *Has2* gene is under the control of the PI3K or Akt pathway, respectively (Fig. 7*G*). These data suggest that Has2 plays a role in the *Smpd3*/nSMase2-mediated inhibition of chondrocyte maturation via PI3K-Akt signaling.

DISCUSSION

Previous reports had suggested that Smpd3/nSMase2 may have a crucial role in *in vivo* chondrogenesis (36–38). We observed a moderate level of *Smpd3* expression in the brains of adult mice (Fig. 1*J*), consistent with the finding that *Smpd3*$^{-/-}$ mice showed a defect in the hypothalamus-pituitary growth axis, which likely accounted for the dwarfism (37). However, the enlarged hypertrophic zone and retarded apoptosis in the chondrocytes of mutant mice cannot be explained by the reduced production of growth hormone and IGF (37). In this study, we present evidence for a cell-autonomous role of the nSMase-ceramide axis in regulating Akt signaling and the subsequent chondrogenic marker expression and differentiation. The induction of *Smpd3* by BMP-2 was a common feature among the tested chondrogenic cells, including primary articular chondrocytes, but *Smpd3* did not seem to be a direct target of the BMP-Smad pathway. Its coding protein, nSMase2, was dominant in mature hypertrophic chondrocytes *in vivo* (Fig. 1*J*), with an expression pattern resembling that of Runx2, whereas the loss of Runx2 suppressed expression of *Smpd3* (Fig. 2, *C*, *D* and *F*). Taken together with the evidence that Runx2 directly interacts with and activates the promoter of *Smpd3* in C2C12 myoblasts (39), Runx2 seems to be mainly responsible for the spatiotemporal expression of *Smpd3* in chondrocytes, in concert with BMP signaling. In addition, it should be noted that the maximum expression of *Smpd3*/nSMase2 *in vivo* was observed in bone tissue, where Runx2 is highly expressed. So far, the molecular mechanism by which BMP-2 increases Runx2-dependent expression of *Smpd3* remains unclear. It is likely that a mechanism similar to that of *Col10a1* gene induction, in which BMP-activated Smads interact with Runx2 to enhance the *Col10a1* promoter-activating ability of Runx2 to drive chondrocyte maturation (13), may take place on the *Smpd3* promoter.

PI3K and its downstream Akt are activated by a large number of receptors, but most notably by tyrosine kinases, such as the IGF-1 receptor. The majority of published studies suggest that PI3K or Akt signaling is required for normal hypertrophic cell maturation and endochondral bone growth during cartilage development (51, 54, 55), although the precise molecular mechanisms for this remain unclear. We demonstrated that the loss

FIGURE 5. **Blocking the Akt or PI3K pathway negates the *Smpd3* siRNA-mediated acceleration of chondrogenesis initiated by BMP-2 in ATDC5 cells.** *A*, ATDC5 cells were transfected with control siRNA (*siCont*) or *Smpd3* siRNA (*siSmpd3*) for 16 h and stimulated by BMP-2 (300 ng/ml) with or without MK2206 at the indicated concentrations (micromolar) for 6 days. Expression of *Smpd3*, *Acan*, *Col2a1*, and *Col10a1* was evaluated by quantitative RT-PCR. *B*, ATDC5 cells were transfected with control siRNA (*siCont*) or *Smpd3* siRNA (*siSmpd3*) for 16 h, and then cultured in the presence of BMP-2 (300 ng/ml) with or without MK2206 (10 μM) for 9 days. Alcian blue staining was performed. *Scale bar*, 300 μm. *C*, ATDC5 cells were transfected with control siRNA (*siCont*) or *Smpd3* siRNA (*siSmpd3*) for 16 h and stimulated by BMP-2 (300 ng/ml) with or without rapamycin at the indicated concentrations (micromolar) for 3 days. Expression of *Smpd3* and *Col10a1* was evaluated by quantitative RT-PCR. *D*, ATDC5 cells were transfected with control siRNA (*siCont*) or *Smpd3* siRNA (*siSmpd3*) for 16 h and stimulated by BMP-2 (300 ng/ml) for 24 h, and then immunoblotted for the indicated antibodies. Tubulin served as a loading control. *E*, ATDC5 cells were transfected with control siRNA (*siCont*) or *Smpd3* siRNA (*siSmpd3*) for 16 h and further stimulated by BMP-2 (300 ng/ml) with or without LY294002 at the indicated concentrations (μM) for 6 days. Expression of *Smpd3*, *Acan*, *Col2a1*, and *Col10a1* was evaluated by quantitative RT-PCR analysis. *F*, mouse primary chondrocytes were transfected with control siRNA (*siCont*) or *Smpd3* siRNA (*siSmpd3*) for 16 h, and were further stimulated by BMP-2 (300 ng/ml) with or without LY294002 (*LY*, 25 μM), MK2206 (*MK*, 5 μM), or rapamycin (*Rp*, 0.5 μM) for 7 days. Expression of *Smpd3*, *Acan*, *Col2a1*, and *Col10a1* was evaluated by quantitative RT-PCR analysis. *, $p < 0.05$; **, $p < 0.01$; *n.s.*, not significant.

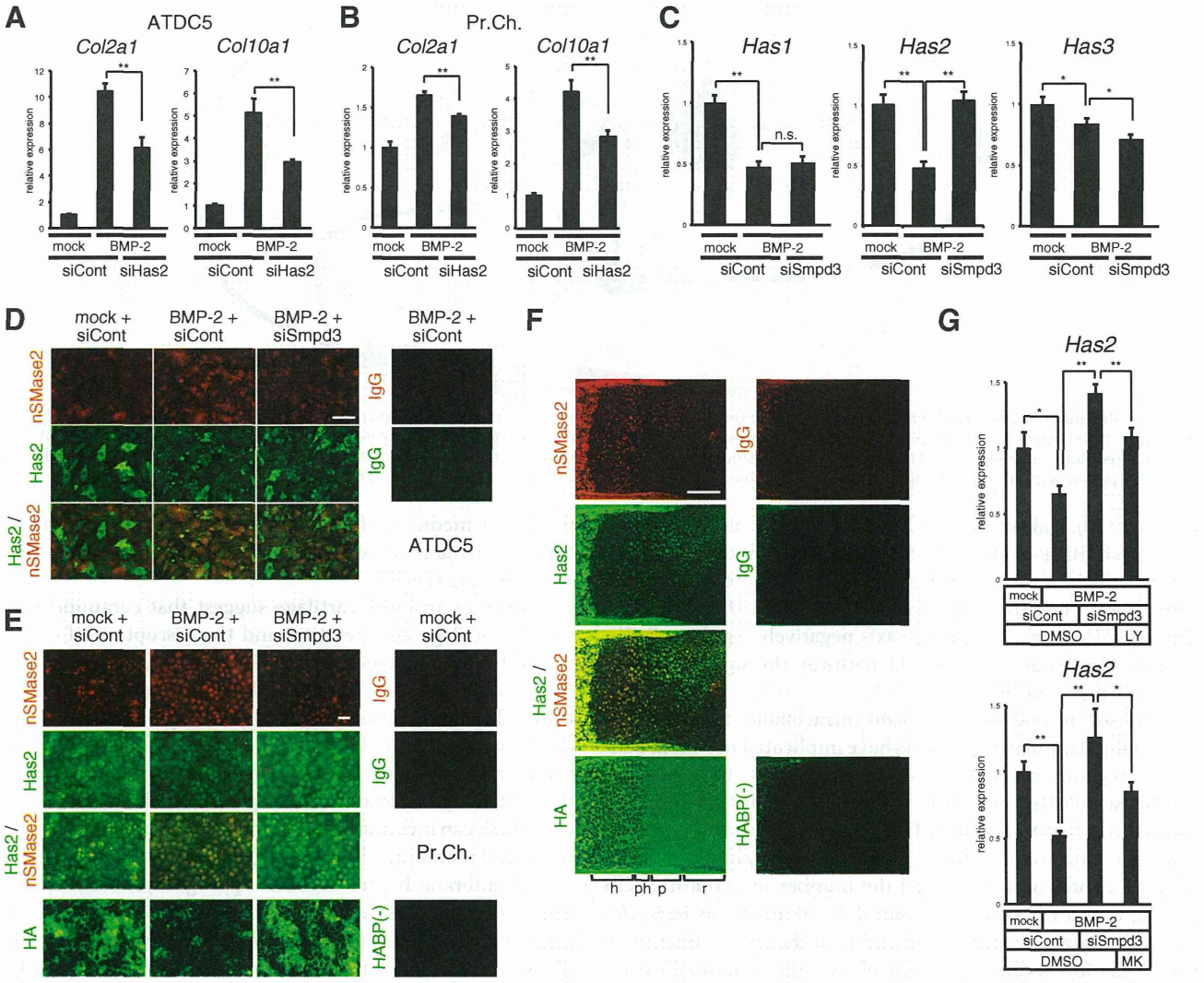

FIGURE 7. **Expression of Has2 is suppressed by nSMase2 via the PI3K or Akt pathway in ATDC5 cells, whereas localization of nSMase2 and Has2 is mutually exclusive in the growth plate cartilage of mouse embryo.** *A* and *B*, ATDC5 cells (*A*) or mouse primary chondrocytes (*B*) were transfected with control siRNA (*siCont*) or *Has2* siRNA (*siHas2*) for 16 h and then treated with BMP-2 (300 ng/ml) for 6 days. Quantitative RT-PCR analysis was performed for *Col2a1* and *Col10a1*. *C*, ATDC5 chondrocytes were transfected with control siRNA (*siCont*) or *Smpd3* siRNA (*siSmpd3*) for 16 h and then treated with BMP-2 (300 ng/ml) for 6 days. Quantitative RT-PCR analysis was performed for *Has1*, *Has2*, and *Has3*. *D*, immunofluorescence for nSMase2 or Has2 was performed in ATDC5 chondrocytes. IgG was used as negative control. *Scale bar,* 50 μm. *E*, immunofluorescence for nSMase2 or Has2 was performed on mouse primary chondrocytes. Biotin-conjugated hyaluronan-binding protein (*HABP*) and Alexa Fluor 488-conjugated streptavidin were applied to detect hyaluronan. IgG was the negative control. *Scale bar,* 50 μm. *F*, expression of nSMase2 or Has2 in mouse E17.5 humerus cartilage was evaluated by immunofluorescence. Biotin-conjugated HA-binding protein and Alexa Fluor 488-conjugated streptavidin were used to detect hyaluronan. IgG was the negative control. *r*, resting chondrocytes; *p*, proliferating chondrocytes; *ph*, prehypertrophic chondrocytes; *h*, hypertrophic chondrocytes. *Scale bar,* 250 μm. *G*, ATDC5 cells were transfected with control siRNA (*siCont*) or *Smpd3* siRNA (*siSmpd3*) for 16 h and further stimulated by BMP-2 (300 ng/ml) with or without LY294002 (*LY*, 1 μM) or MK2206 (*MK*, 1 μM) for 6 days. Expression of *Has2* was evaluated by quantitative RT-PCR analysis. *, $p < 0.05$; **, $p < 0.01$; *n.s.*, not significant.

or gain of *Smpd3*/nSMase2 function in chondrocytes increased or decreased the phosphorylation of both PI3K and Akt, respectively. In an RTK signaling antibody array, only phosphorylation of Akt and rpS6 was strengthened by the loss of *Smpd3* (Fig. 4*A*), demonstrating their specificity as downstream targets of nSMase2. Importantly, the increase in Akt phosphorylation was induced by the addition of BMP-2 and not by ITS alone (Fig. 4, *A*, *D* and *E*). A similar enhancement in the phosphorylation of Akt was observed within 1 h of BMP-2 application in gastric cancer cells, although the precise mechanism by which the BMP-2 signaling pathway induced Akt activity was unclear (56). We expect the Akt pathway to take part in BMP-2-induced chondrogenesis because this pathway promotes chondrocyte differentiation.

The GW4869-mediated blockade of nSMase2 function accelerated differentiation of ATDC5 chondrocytes, as well as hypertrophic conversion and calcification of chondrocytes, in bone *ex vivo* culture; both phenotypes were cancelled by application of C_2-ceramide (Figs. 3*C* and 6, *A* and *B*). nSMase2 hydrolyzes the phosphodiester bond of the membrane sphingolipid sphingomyelin to yield ceramide and phosphocholine (57). Ceramides have been shown to reduce the level of Akt phosphorylation by activating protein phosphatase 2A (PP2A) (58). The phosphorylation level of PP2A in *fro*/*fro* fibroblasts is

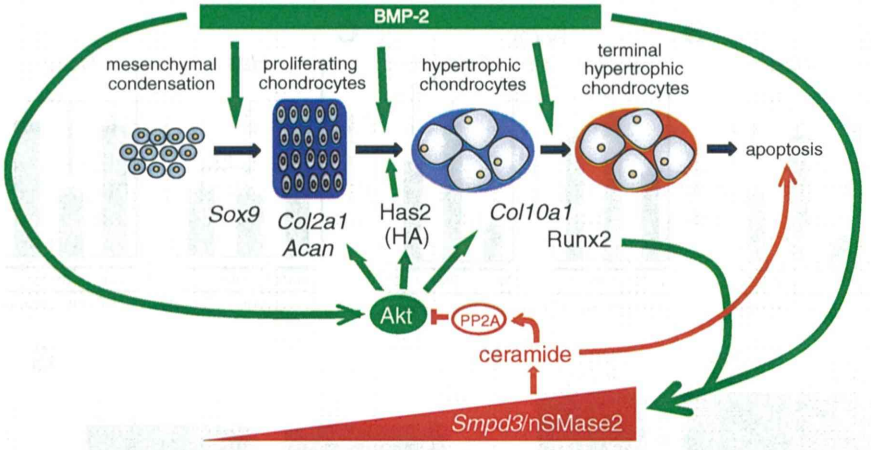

FIGURE 8. **Proposed model for the negative or positive regulation of chondrocyte maturation or apoptosis by *Smpd3*/nSMase2, respectively.** BMP-2 promotes chondrogenesis by multiple pathways, including activation of Akt signaling and the subsequent induction of Has2. During chondrocyte maturation, up-regulated Runx2 induces *Smpd3* in concert with BMP signaling. nSMase2 releases ceramide, which activates PP2A to dephosphorylate Akt. This blockade of the Akt pathway interferes not only with chondrocyte maturation but also with Has2-mediated production of HA.

reduced (50). Taken together, in the maturing phase of chondrogenesis, BMP-2-induced nSMase2 is thought to release ceramide, which in turn activates PP2A to inactivate Akt and the subsequent chondrogenic molecular cascades (Fig. 8). Thus, the *Smpd3*/nSMase2-ceramide axis negatively regulates BMP-2-induced activation of the Akt pathway through a negative feedback mechanism.

nSMase2 is one of the major intracellular regulators of sphingolipids, and many reports have implicated nSMase2 activation in ceramide-mediated apoptosis (49, 59–61). Sphingomyelinase-released ceramide is essential for the clustering of the death receptors CD95 or DR5 in membrane rafts to trigger apoptosis (62, 63). Indeed, silencing of *Smpd3* in mature ATDC5 chondrocytes reduced the number of apoptotic cells (Fig. 6, *C* and *D*), suggesting that delayed apoptosis in *fro/fro* cartilage was a cell-autonomous effect of the loss of function of nSMase2 (36). Because apoptosis of terminally matured hypertrophic chondrocytes is a crucial step in the transition of chondrogenic stage to the bone formation stage in the endochondral ossification system, *Smpd3*/nSMase2 probably plays a key role in regulating the timing of osteogenesis onset.

HA is a linear high molecular weight glycosaminoglycan and is composed of disaccharide repeats of glucuronic acid and *N*-acetylglucosamine. It is produced in the plasma membrane by three hyaluronan synthases (Has1–3); Has2 is the crucial hyaluronan synthase involved in the endochondral ossification process (53). The Akt-rpS6 pathway is important in the expression of *Has2* in MCF-7 breast cancer cells (64), although nSMase2 suppresses production of Has2 via inactivation of Akt in mouse dermal fibroblasts (50). In chondrocytes, Has2 expression was decreased by BMP-2 stimulation and was then recovered by silencing of *Smpd3*, demonstrating the importance of BMP-induced *Smpd3*/nSMase2 in the suppression of Has2 (Fig. 7, *C–E*). Because an inhibitor compound for PI3K or Akt cancelled this effect (Fig. 7*G*), *Has2* expression is also considered to be under the control of PI3K-Akt signaling. *In vivo*, expression of Has2 was diminished in hypertrophic chondrocytes, whereas nSMase2 was strongly expressed in the same cells (Fig. 7*F*). Taken together, these results indicate that Has2 is another mediator of *Smpd3*/nSMase2-induced inhibition of the hypertrophic maturation of chondrocytes, downstream of Akt signaling (Fig. 8).

Studies of articular cartilage suggest that ceramide plays a role in cartilage degeneration and the disruption of cartilage matrix homeostasis to decrease the levels of type II collagen (65, 66). Farber disease, in which a lack of ceramidase causes excess ceramide accumulation within the cartilage and bone, is associated with arthritis-like joint degeneration (67). Moreover, tumor necrosis factor α (TNFα), a proinflammatory cytokine that is widely implicated in the pathogenesis of arthritic diseases (68), can increase the level of ceramide through hydrolysis of the cell membrane lipid sphingomyelin by endosomal acidic and membrane-bound neutral sphingomyelinases (69). In chondrocytes, we observed a decrease of *Col2a1* expression by induction of C^2-ceramide or *Smpd3*-expressing adenovirus. Conversely, *Smpd3* knock-out mice showed an enlarged hypertrophic zone in the growth plate of the joints and, in adulthood, a severe OA-phenotype with osteophytes in the knee joint (38). Similarly, in chondrocytes, we observed increase of hypertrophic phenotype (*Col10a1*) by induction of *Smpd3* siRNA. Accordingly, an excess level of nSMase2 leads to the degradation of cartilage matrix proteins, whereas loss of nSMase2 introduces a hypertrophic change in chondrocytes, and both circumstances may result in the progression of OA. Therefore, the expression of *Smpd3*/nSMase2 must be fine-tuned to maintain cartilage homeostasis that is, at least in part, controlled by Runx2 and BMP signaling.

In the case of cartilage regenerative medicine, pharmacological manipulation of steps of the nSMase2-ceramide-PP2A-Akt pathway may improve the efficiency and quality of generated tissues. As an indication, it is noteworthy that we could manipulate hypertrophic conversion and calcification in *ex vivo* cartilage rudiment culture using combinations of BMP-2, GW4869, and C_2-ceramide (Fig. 6, *A* and *B*).

In summary, our study has provided a cell-autonomous pivotal role for *Smpd3*/nSMase2 in determining the rate of chondrocyte maturation in chondrocytes. As illustrated in Fig. 8, BMP-2 accelerates general chondrogenesis through multiple

approaches, including activation of the Akt pathway, which involves induction of *Has2* and a subsequent production of HA. Meanwhile, increased Runx2 in maturating chondrocytes induces *Smpd3* in concert with BMP-2. nSMase2, coded by *Smpd3*, releases ceramide from the cell membrane to activate PP2A, which in turn dephosphorylates Akt. This inactivation of the Akt pathway suppresses not only chondrocyte differentiation and subsequent maturation but also production of HA via Has2. We propose that *Smpd3*/nSMase2 is a molecular target in cartilage and bone medicine that constitutes a negative feedback loop in BMP-induced chondrogenesis.

Acknowledgments—Human chondrocyte C28/I2 was kindly provided by Dr. Mary Goldring. We gratefully acknowledge the technical assistance of Hui Gao.

REFERENCES

1. Bi, W., Deng, J. M., Zhang, Z., Behringer, R. R., and de Crombrugghe, B. (1999) Sox9 is required for cartilage formation. *Nat. Genet.* **22,** 85–89
2. Akiyama, H., Chaboissier, M. C., Martin, J. F., Schedl, A., and de Crombrugghe, B. (2002) The transcription factor Sox9 has essential roles in successive steps of the chondrocyte differentiation pathway and is required for expression of Sox5 and Sox6. *Genes Dev.* **16,** 2813–2828
3. Provot, S., and Schipani, E. (2005) Molecular mechanisms of endochondral bone development. *Biochem. Biophys. Res. Commun.* **328,** 658–665
4. Enomoto, H., Enomoto-Iwamoto, M., Iwamoto, M., Nomura, S., Himeno, M., Kitamura, Y., Kishimoto, T., and Komori, T. (2000) Cbfa1 is a positive regulatory factor in chondrocyte maturation. *J. Biol. Chem.* **275,** 8695–8702
5. Zheng, Q., Zhou, G., Morello, R., Chen, Y., Garcia-Rojas, X., and Lee, B. (2003) Type X collagen gene regulation by Runx2 contributes directly to its hypertrophic chondrocyte-specific expression *in vivo*. *J. Cell Biol.* **162,** 833–842
6. Kronenberg, H. M. (2003) Developmental regulation of the growth plate. *Nature* **423,** 332–336
7. Miyazono, K., Maeda, S., and Imamura, T. (2005) BMP receptor signaling: transcriptional targets, regulation of signals, and signaling cross-talk. *Cytokine Growth Factor Rev.* **16,** 251–263
8. Guo, X., and Wang, X. F. (2009) Signaling cross-talk between TGF-β/BMP and other pathways. *Cell Res.* **19,** 71–88
9. Pogue, R., and Lyons, K. (2006) BMP signaling in the cartilage growth plate. *Curr. Top. Dev. Biol.* **76,** 1–48
10. Hatakeyama, Y., Tuan, R. S., and Shum, L. (2004) Distinct functions of BMP4 and GDF5 in the regulation of chondrogenesis. *J. Cell. Biochem.* **91,** 1204–1217
11. Haas, A. R., and Tuan, R. S. (1999) Chondrogenic differentiation of murine C3H10T1/2 multipotential mesenchymal cells: II. Stimulation by bone morphogenetic protein-2 requires modulation of N-cadherin expression and function. *Differentiation* **64,** 77–89
12. Fujii, M., Takeda, K., Imamura, T., Aoki, H., Sampath, T. K., Enomoto, S., Kawabata, M., Kato, M., Ichijo, H., and Miyazono, K. (1999) Roles of bone morphogenetic protein type I receptors and Smad proteins in osteoblast and chondroblast differentiation. *Mol. Biol. Cell* **10,** 3801–3813
13. Leboy, P., Grasso-Knight, G., D'Angelo, M., Volk, S. W., Lian, J. V., Drissi, H., Stein, G. S., and Adams, S. L. (2001) Smad-Runx interactions during chondrocyte maturation. *J. Bone Joint Surg. Am.* **83,** S15–S22
14. Valcourt, U., Gouttenoire, J., Moustakas, A., Herbage, D., and Mallein-Gerin, F. (2002) Functions of transforming growth factor-β family type I receptors and Smad proteins in the hypertrophic maturation and osteoblastic differentiation of chondrocytes. *J. Biol. Chem.* **277,** 33545–33558
15. Tsumaki, N., Nakase, T., Miyaji, T., Kakiuchi, M., Kimura, T., Ochi, T., and Yoshikawa, H. (2002) Bone morphogenetic protein signals are required for cartilage formation and differently regulate joint development during skeletogenesis. *J. Bone Miner. Res.* **17,** 898–906
16. Yoon, B. S., Ovchinnikov, D. A., Yoshii, I., Mishina, Y., Behringer, R. R., and Lyons, K. M. (2005) Bmpr1a and Bmpr1b have overlapping functions and are essential for chondrogenesis *in vivo*. *Proc. Natl. Acad. Sci. U.S.A.* **102,** 5062–5067
17. Retting, K. N., Song, B., Yoon, B. S., and Lyons, K. M. (2009) BMP canonical Smad signaling through Smad1 and Smad5 is required for endochondral bone formation. *Development* **136,** 1093–1104
18. Volk, S. W., Luvalle, P., Leask, T., and Leboy, P. S. (1998) A BMP-responsive transcriptional region in the chicken type X collagen gene. *J. Bone Miner. Res.* **13,** 1521–1529
19. Kempf, H., Ionescu, A., Udager, A. M., and Lassar, A. B. (2007) Prochondrogenic signals induce a competence for Runx2 to activate hypertrophic chondrocyte gene expression. *Dev. Dyn.* **236,** 1954–1962
20. Kobayashi, T., Lyons, K. M., McMahon, A. P., and Kronenberg, H. M. (2005) BMP signaling stimulates cellular differentiation at multiple steps during cartilage development. *Proc. Natl. Acad. Sci. U.S.A.* **102,** 18023–18027
21. Scotti, C., Tonnarelli, B., Papadimitropoulos, A., Scherberich, A., Schaeren, S., Schauerte, A., Lopez-Rios, J., Zeller, R., Barbero, A., and Martin, I. (2010) Recapitulation of endochondral bone formation using human adult mesenchymal stem cells as a paradigm for developmental engineering. *Proc. Natl. Acad. Sci. U.S.A.* **107,** 7251–7256
22. Pullig, O., Weseloh, G., Ronneberger, D., Käkönen, S., and Swoboda, B. (2000) Chondrocyte differentiation in human osteoarthritis: expression of osteocalcin in normal and osteoarthritic cartilage and bone. *Calcif. Tissue Int.* **67,** 230–240
23. Sandell, L. J., and Aigner, T. (2001) Articular cartilage and changes in arthritis. An introduction: cell biology of osteoarthritis. *Arthritis Res.* **3,** 107–113
24. Dreier, R. (2010) Hypertrophic differentiation of chondrocytes in osteoarthritis: The developmental aspect of degenerative joint disorders. *Arthritis Res. Ther.* **12,** 216
25. Nelea, V., Luo, L., Demers, C. N., Antoniou, J., Petit, A., Lerouge, S., R Wertheimer, M., and Mwale, F. (2005) Selective inhibition of type X collagen expression in human mesenchymal stem cell differentiation on polymer substrates surface-modified by glow discharge plasma. *J. Biomed. Mater. Res. A* **75,** 216–223
26. Sekiya, I., Vuoristo, J. T., Larson, B. L., and Prockop, D. J. (2002) *In vitro* cartilage formation by human adult stem cells from bone marrow stroma defines the sequence of cellular and molecular events during chondrogenesis. *Proc. Natl. Acad. Sci. U.S.A.* **99,** 4397–4402
27. Imamura, T., Takase, M., Nishihara, A., Oeda, E., Hanai, J., Kawabata, M., and Miyazono, K. (1997) Smad6 inhibits signalling by the TGF-β superfamily. *Nature* **389,** 622–626
28. Zhu, H., Kavsak, P., Abdollah, S., Wrana, J. L., and Thomsen, G. H. (1999) A SMAD ubiquitin ligase targets the BMP pathway and affects embryonic pattern formation. *Nature* **400,** 687–693
29. Murakami, G., Watabe, T., Takaoka, K., Miyazono, K., and Imamura, T. (2003) Cooperative inhibition of bone morphogenetic protein signaling by Smurf1 and inhibitory Smads. *Mol. Biol. Cell* **14,** 2809–2817
30. Kawamura, I., Maeda, S., Imamura, K., Setoguchi, T., Yokouchi, M., Ishidou, Y., and Komiya, S. (2012) SnoN suppresses maturation of chondrocytes by mediating signal cross-talk between transforming growth factor-β and bone morphogenetic protein pathways. *J. Biol. Chem.* **287,** 29101–29113
31. Obeid, L. M., Linardic, C. M., Karolak, L. A., and Hannun, Y. A. (1993) Programmed cell death induced by ceramide. *Science* **259,** 1769–1771
32. Sjöholm, A. (1995) Ceramide inhibits pancreatic β-cell insulin production and mitogenesis and mimics the actions of interleukin-1 β. *FEBS Lett.* **367,** 283–286
33. Mebarek, S., Komati, H., Naro, F., Zeiller, C., Alvisi, M., Lagarde, M., Prigent, A. F., and Némoz, G. (2007) Inhibition of *de novo* ceramide synthesis upregulates phospholipase D and enhances myogenic differentiation. *J. Cell Sci.* **120,** 407–416
34. Sharma, K., and Shi, Y. (1999) The yins and yangs of ceramide. *Cell Res.* **9,** 1–10
35. Aubin, I., Adams, C. P., Opsahl, S., Septier, D., Bishop, C. E., Auge, N., Salvayre, R., Negre-Salvayre, A., Goldberg, M., Guénet, J. L., and Poirier, C.

(2005) A deletion in the gene encoding sphingomyelin phosphodiesterase 3 (Smpd3) results in osteogenesis and dentinogenesis imperfecta in the mouse. *Nat. Genet.* **37,** 803–805
36. Khavandgar, Z., Poirier, C., Clarke, C. J., Li, J., Wang, N., McKee, M. D., Hannun, Y. A., and Murshed, M. (2011) A cell-autonomous requirement for neutral sphingomyelinase 2 in bone mineralization. *J. Cell Biol.* **194,** 277–289
37. Stoffel, W., Jenke, B., Blöck, B., Zumbansen, M., and Koebke, J. (2005) Neutral sphingomyelinase 2 (smpd3) in the control of postnatal growth and development. *Proc. Natl. Acad. Sci. U.S.A.* **102,** 4554–4559
38. Stoffel, W., Jenke, B., Holz, B., Binczek, E., Günter, R. H., Knifka, J., Koebke, J., and Niehoff, A. (2007) Neutral sphingomyelinase (SMPD3) deficiency causes a novel form of chondrodysplasia and dwarfism that is rescued by Col2A1-driven smpd3 transgene expression. *Am. J. Pathol.* **171,** 153–161
39. Chae, Y. M., Heo, S. H., Kim, J. Y., Lee, J. M., Ryoo, H. M., and Cho, J. Y. (2009) Upregulation of smpd3 via BMP2 stimulation and Runx2. *BMB Rep.* **42,** 86–90
40. Atsumi, T., Miwa, Y., Kimata, K., and Ikawa, Y. (1990) A chondrogenic cell line derived from a differentiating culture of AT805 teratocarcinoma cells. *Cell Differ. Dev.* **30,** 109–116
41. Goldring, M. B., Birkhead, J. R., Suen, L. F., Yamin, R., Mizuno, S., Glowacki, J., Arbiser, J. L., and Apperley, J. F. (1994) Interleukin-1 β-modulated gene expression in immortalized human chondrocytes. *J. Clin. Invest.* **94,** 2307–2316
42. Alvarez, J., Sohn, P., Zeng, X., Doetschman, T., Robbins, D. J., and Serra, R. (2002) TGFβ2 mediates the effects of hedgehog on hypertrophic differentiation and PTHrP expression. *Development* **129,** 1913–1924
43. Shukunami, C., Ohta, Y., Sakuda, M., and Hiraki, Y. (1998) Sequential progression of the differentiation program by bone morphogenetic protein-2 in chondrogenic cell line ATDC5. *Exp. Cell Res.* **241,** 1–11
44. Yao, Y., and Wang, Y. (2013) ATDC5: an excellent *in vitro* model cell line for skeletal development. *J. Cell. Biochem.* **114,** 1223–1229
45. Origuchi, N., Ishidou, Y., Nagamine, T., Onishi, T., Matsunaga, S., Yoshida, H., and Sakou, T. (1998) The spatial and temporal immunolocalization of TGF-β 1 and bone morphogenetic protein-2/-4 in phallic bone formation in inbred Sprague Dawley male rats. *In Vivo* **12,** 473–480
46. Heinonen, J., Taipaleenmäki, H., Roering, P., Takatalo, M., Harkness, L., Sandholm, J., Uusitalo-Järvinen, H., Kassem, M., Kiviranta, I., Laitala-Leinonen, T., and Säämänen, A. M. (2011) Snorc is a novel cartilage specific small membrane proteoglycan expressed in differentiating and articular chondrocytes. *Osteoarthritis Cartilage* **19,** 1026–1035
47. Korchynskyi, O., and ten Dijke, P. (2002) Identification and functional characterization of distinct critically important bone morphogenetic protein-specific response elements in the Id1 promoter. *J. Biol. Chem.* **277,** 4883–4891
48. Lefebvre, V., Li, P., and de Crombrugghe, B. (1998) A new long form of Sox5 (L-Sox5), Sox6 and Sox9 are coexpressed in chondrogenesis and cooperatively activate the type II collagen gene. *EMBO J.* **17,** 5718–5733
49. Marchesini, N., Luberto, C., and Hannun, Y. A. (2003) Biochemical properties of mammalian neutral sphingomyelinase 2 and its role in sphingolipid metabolism. *J. Biol. Chem.* **278,** 13775–13783
50. Qin, J., Berdyshev, E., Poirer, C., Schwartz, N. B., and Dawson, G. (2012) Neutral sphingomyelinase 2 deficiency increases hyaluronan synthesis by up-regulation of hyaluronan synthase 2 through decreased ceramide production and activation of Akt. *J. Biol. Chem.* **287,** 13620–13632
51. Rokutanda, S., Fujita, T., Kanatani, N., Yoshida, C. A., Komori, H., Liu, W., Mizuno, A., and Komori, T. (2009) Akt regulates skeletal development through GSK3, mTOR, and FoxOs. *Dev. Biol.* **328,** 78–93
52. Shukunami, C., Shigeno, C., Atsumi, T., Ishizeki, K., Suzuki, F., and Hiraki, Y. (1996) Chondrogenic differentiation of clonal mouse embryonic cell line ATDC5 *in vitro*: differentiation-dependent gene expression of parathyroid hormone (PTH)/PTH-related peptide receptor. *J. Cell Biol.* **133,** 457–468
53. Matsumoto, K., Li, Y., Jakuba, C., Sugiyama, Y., Sayo, T., Okuno, M., Dealy, C. N., Toole, B. P., Takeda, J., Yamaguchi, Y., and Kosher, R. A. (2009) Conditional inactivation of Has2 reveals a crucial role for hyaluronan in skeletal growth, patterning, chondrocyte maturation and joint formation in the developing limb. *Development* **136,** 2825–2835
54. Ulici, V., Hoenselaar, K. D., Gillespie, J. R., and Beier, F. (2008) The PI3K pathway regulates endochondral bone growth through control of hypertrophic chondrocyte differentiation. *BMC Dev. Biol.* **8,** 40
55. Fujita, T., Azuma, Y., Fukuyama, R., Hattori, Y., Yoshida, C., Koida, M., Ogita, K., and Komori, T. (2004) Runx2 induces osteoblast and chondrocyte differentiation and enhances their migration by coupling with PI3K-Akt signaling. *J. Cell Biol.* **166,** 85–95
56. Kang, M. H., Kim, J. S., Seo, J. E., Oh, S. C., and Yoo, Y. A. (2010) BMP2 accelerates the motility and invasiveness of gastric cancer cells via activation of the phosphatidylinositol 3-kinase (PI3K)/Akt pathway. *Exp. Cell Res.* **316,** 24–37
57. Bartke, N., and Hannun, Y. A. (2009) Bioactive sphingolipids: metabolism and function. *J. Lipid Res.* **50,** S91–S96
58. Mora, A., Sabio, G., Risco, A. M., Cuenda, A., Alonso, J. C., Soler, G., and Centeno, F. (2002) Lithium blocks the PKB and GSK3 dephosphorylation induced by ceramide through protein phosphatase-2A. *Cell. Signal.* **14,** 557–562
59. Kolesnick, R., and Hannun, Y. A. (1999) Ceramide and apoptosis. *Trends Biochem. Sci.* **24,** 224–225
60. Wiesner, D. A., Kilkus, J. P., Gottschalk, A. R., Quintáns, J., and Dawson, G. (1997) Anti-immunoglobulin-induced apoptosis in WEHI 231 cells involves the slow formation of ceramide from sphingomyelin and is blocked by bcl-XL. *J. Biol. Chem.* **272,** 9868–9876
61. Lee, J. T., Xu, J., Lee, J. M., Ku, G., Han, X., Yang, D. I., Chen, S., and Hsu, C. Y. (2004) Amyloid-β peptide induces oligodendrocyte death by activating the neutral sphingomyelinase-ceramide pathway. *J. Cell Biol.* **164,** 123–131
62. Grassme, H., Jekle, A., Riehle, A., Schwarz, H., Berger, J., Sandhoff, K., Kolesnick, R., and Gulbins, E. (2001) CD95 signaling via ceramide-rich membrane rafts. *J. Biol. Chem.* **276,** 20589–20596
63. Dumitru, C. A., and Gulbins, E. (2006) TRAIL activates acid sphingomyelinase via a redox mechanism and releases ceramide to trigger apoptosis. *Oncogene* **25,** 5612–5625
64. Kultti, A., Kärnä, R., Rilla, K., Nurminen, P., Koli, E., Makkonen, K. M., Si, J., Tammi, M. I., and Tammi, R. H. (2010) Methyl-β-cyclodextrin suppresses hyaluronan synthesis by down-regulation of hyaluronan synthase 2 through inhibition of Akt. *J. Biol. Chem.* **285,** 22901–22910
65. Sabatini, M., Rolland, G., Léonce, S., Thomas, M., Lesur, C., Pérez, V., de Nanteuil, G., and Bonnet, J. (2000) Effects of ceramide on apoptosis, proteoglycan degradation, and matrix metalloproteinase expression in rabbit articular cartilage. *Biochem. Biophys. Res. Commun.* **267,** 438–444
66. Gilbert, S. J., Blain, E. J., Jones, P., Duance, V. C., and Mason, D. J. (2006) Exogenous sphingomyelinase increases collagen and sulphated glycosaminoglycan production by primary articular chondrocytes: an *in vitro* study. *Arthritis Res. Ther.* **8,** R89
67. Ehlert, K., Frosch, M., Fehse, N., Zander, A., Roth, J., and Vormoor, J. (2007) Farber disease: clinical presentation, pathogenesis and a new approach to treatment. *Pediatr. Rheumatol. Online J.* **5,** 15
68. Goldring, M. B. (1999) The role of cytokines as inflammatory mediators in osteoarthritis: lessons from animal models. *Connect. Tissue Res.* **40,** 1–11
69. Wiegmann, K., Schütze, S., Machleidt, T., Witte, D., and Krönke, M. (1994) Functional dichotomy of neutral and acidic sphingomyelinases in tumor necrosis factor signaling. *Cell* **78,** 1005–1015

Journal of Gastroenterology and Hepatology

JGHF

doi:10.1111/jgh.12551

GASTROENTEROLOGY

Decreased density of CD3+ tumor-infiltrating lymphocytes during gastric cancer progression

Takaaki Arigami,* Yoshikazu Uenosono,† Sumiya Ishigami,* Daisuke Matsushita,* Tetsushi Hirahara,* Shigehiro Yanagita,* Hiroshi Okumura,* Yasuto Uchikado,* Akihiro Nakajo,* Yuko Kijima* and Shoji Natsugoe*,†

*Department of Digestive Surgery, Breast and Thyroid Surgery, Field of Oncology, and †Molecular Frontier Surgery, Course of Advanced Therapeutics, Kagoshima University Graduate School of Medical and Dental Sciences, Kagoshima, Japan

Key words
CD3, gastric cancer, tumor-infiltrating lymphocytes.

Accepted for publication 28 January 2014.

Correspondence
Dr Takaaki Arigami, Department of Surgical Oncology and Digestive Surgery, Field of Oncology, Course of Advanced Therapeutics, Kagoshima University Graduate School of Medical and Dental Sciences, 8-35-1 Sakuragaoka, Kagoshima 890-8520, Japan.
Email: arigami@m.kufm.kagoshima-u.ac.jp

Conflicts of interest: The authors have no conflict of interest.

Abstract

Background and Aim: Tumor cells escape host immunosurveillance and thus produce an advantageous environment for tumor progression. Recent studies have demonstrated that tumor-infiltrating lymphocytes (TILs) play a principal role in the immune response to tumors. However, little is understood about numerical alterations in CD3+ TILs during tumor progression in patients with gastric cancer. The present study examines the density of CD3+ TILs to elucidate their clinical significance in gastric cancer.

Methods: The numbers of CD3+ TILs in 120 resected specimens from patients with gastric cancer and 27 endoscopic resected specimens from patients with gastric adenoma were immunohistochemically assessed using a CD3 polyclonal antibody.

Results: The mean number of CD3+ TILs (± SD) in the patients with gastric cancer and adenoma was 87.5 ± 59.8 and 379.6 ± 128.1, respectively. Significantly more CD3+ TILs were found in specimens from patients with gastric adenoma than with gastric cancer ($P < 0.0001$). The numbers of CD3+ TILs significantly correlated with depth of tumor invasion, lymph node metastasis, and stage ($P = 0.022$, $P = 0.0004$, and $P = 0.011$, respectively). The 5-year survival rate was significantly poorer for patients with fewer CD3+ TILs ($P = 0.004$). Multivariate analysis selected the density of CD3+ TILs as an independent prognostic factor ($P = 0.034$).

Conclusions: Our results demonstrated that the density of CD3+ TILs decreases during tumor progression. The density of CD3+ TILs is an immunological predictor of lymph node metastasis and disease outcome in patients with gastric cancer.

Introduction

Despite the remarkable development of anticancer agents including novel molecular targeted drugs such as trastuzumab for chemotherapy against gastric cancer, patients with unresectable advanced or recurrent gastric cancer have a poor prognosis. In fact, the 5-year survival rates of patients with stage IIIA, IIIB, and IV gastric cancers are 30.8–54.0%, 16.1–36.5%, and 9.2–23.9%, respectively.[1,2] Such aggressiveness results in gastric tumor cells frequently metastasizing to regional lymph nodes. Lymph node metastasis is an important prognostic factor for patients with gastric cancer.[3–5] Therefore, lymph node recurrence is an important issue in the control of postoperative disease aggressiveness in such patients. Although computed tomography and positron emission tomography have been used to identify lymph node recurrence during the postoperative follow up of patients with gastric cancer, these modalities are of little value to clinical management. To date, several biomarkers have been investigated to predict lymph node status and patients at high risk for recurrent gastric cancer in lymph nodes. However, few molecular biomarkers can actually achieve this.

Host immunosurveillance plays an important role in patients with various malignant neoplasms, including gastric cancer. In particular, the T-cell-mediated immune response controls this surveillance system to prevent tumor progression. Several investigators have recently demonstrated a correlation between tumor-infiltrating lymphocytes (TILs) and disease outcomes in patients with malignant neoplasms.[6–16] Consequently, they reported that TILs could play an important role as a prognostic marker of various malignancies.[6–16] Although CD3 is an established total T-cell marker, higher numbers of CD3+ TILs have been associated with a favorable prognosis in patients with several malignancies such as ovarian, colorectal, and esophageal cancers.[12–15] However, changes in the numbers of CD3+ TILs during tumor progression in patients with gastric cancer have not been studied in detail.

© 2014 Journal of Gastroenterology and Hepatology Foundation and Wiley Publishing Asia Pty Ltd

The present study aims to elucidate the clinical significance of changes in CD3+ TIL density during tumor progression in patients with gastric cancer.

Methods

Patients. The present study enrolled 120 patients (74 men and 46 women; age, 31–83 years; mean, 65 years) with gastric cancer who had been treated by curative gastrectomy with lymphadenectomy at Kagoshima University Hospital (Kagoshima, Japan) between 2000 and 2005. Patients who underwent endoscopic mucosal resection, palliative resection, preoperative chemotherapy, and/or radiation therapy were excluded. None of the enrolled patients had synchronous or metachronous cancer in other organs. The tumors were classified and staged based on the criteria for the tumor-node-metastasis (TNM) classification of gastric carcinoma established by the International Union Against Cancer (UICC).[17] Table 1 shows the UICC stage and clinicopathological characteristics of patients enrolled in this study. All patients were followed up every 3–6 months by regular clinical examinations including tumor marker studies (carcinoembryonic antigen and carbohydrate antigen 19-9), radiography, ultrasonography, and computed tomography at Kagoshima University Hospital. The median post-surgical follow-up period was 36 months (range, 1–112 months). We compared the density of CD3+ TILs between gastric cancer and 27 gastric adenoma specimens obtained by endoscopic resection. Resected gastric tumors were fixed with 10% formalin in phosphate-buffered saline (PBS), embedded in paraffin and sectioned (paraffin-embedded archival tumors [PEAT]) into 3 μm slices for immunohistochemical analysis.

This Ethics Committee of the Kagoshima University approved the study and all patients provided written informed consent to the use of their information.

Table 1 Clinicopathological characteristics of 120 patients with gastric cancer

Sex	
Male	74
Female	46
Age (year)	
≤ 70	72
> 70	48
Histological type	
Differentiated	50
Undifferentiated	70
Depth of tumor invasion	
pT1	44
pT2	5
pT3	34
pT4	37
Lymph node metastasis	
N0	54
N1	11
N2	17
N3	38
Stage	
I	46
II	16
III	36
IV	22
Lymphatic invasion	
Negative	40
Positive	80
Venous invasion	
Negative	58
Positive	62

Immunohistochemistry. Paraffin-embedded archival gastric tumor sections (3 μm thick) incubated on slides at 50°C overnight were deparaffinized with xylene and then rehydrated with a graded series of ethanol. The sections were washed in PBS and then incubated in DakoCytomation Proteinase K (DAKO Corporation, Carpinteria, CA, USA) at room temperature for 10 min to activate the antigen. Endogenous peroxidase activity was blocked using Peroxidase Blocking Reagent (DAKO) for 10 min after cooling at room temperature. Non-specific binding was blocked at room temperature for 30 min with Protein Block Serum-Free Reagent (DAKO). The sections were washed in PBS, incubated at room temperature for 60 min with anti-human CD3 antibody (DAKO) diluted 1:100 in Dako antibody diluent with background-reducing components (DAKO). Reactions for CD3 were developed using Vectastain ABC kits (Vector Laboratories Inc., Burlingame, CA, USA) and visualized using diaminobenzidine tetrahydrochloride.[18]

Quantitation of CD3+ TILs. All slides were independently assessed by two investigators (T.A. and Y.U.) who were blinded to the clinicopathological data of the patients. The CD3+ TILs were quantified based on established density criteria.[19,20] Specifically, each investigator selected five fields in tumor foci with the highest intensity of CD3+ TILs at low magnification (×40). The CD3+ TILs were counted and recorded at higher magnification (×200). The number of CD3+ TILs was averaged and used in the statistical analysis.

Statistical analysis. Differences in the density of CD3+ TILs between patients with gastric cancer and with gastric adenoma, and the relationship between the number of CD3+ TILs and categorical clinicopathological factors were assessed using the Wilcoxon rank sum test. Relationships between the density of CD3+ TILs and several factors, such as depth of tumor invasion, stage, and lymph node status classified based on the criteria for the TNM classification of UICC as N0 versus N1 versus N2 versus N3, were assessed using the Kruskal–Wallis test. Receiver operating characteristic (ROC) curves were constructed and then the predictive power of CD3+ TIL density to detect patients with lymph node metastasis was assessed from the area under the curve (AUC). Kaplan–Meier survival curves were generated and differences in survival were determined using the log-rank test. Prognostic factors were assessed by univariate and multivariate analyses (Cox proportional hazards regression model). All data were statistically analyzed using SAS statistical software (SAS Institute Inc., Cary, NC, USA). A P value of < 0.05 was considered statistically significant.

© 2014 Journal of Gastroenterology and Hepatology Foundation and Wiley Publishing Asia Pty Ltd

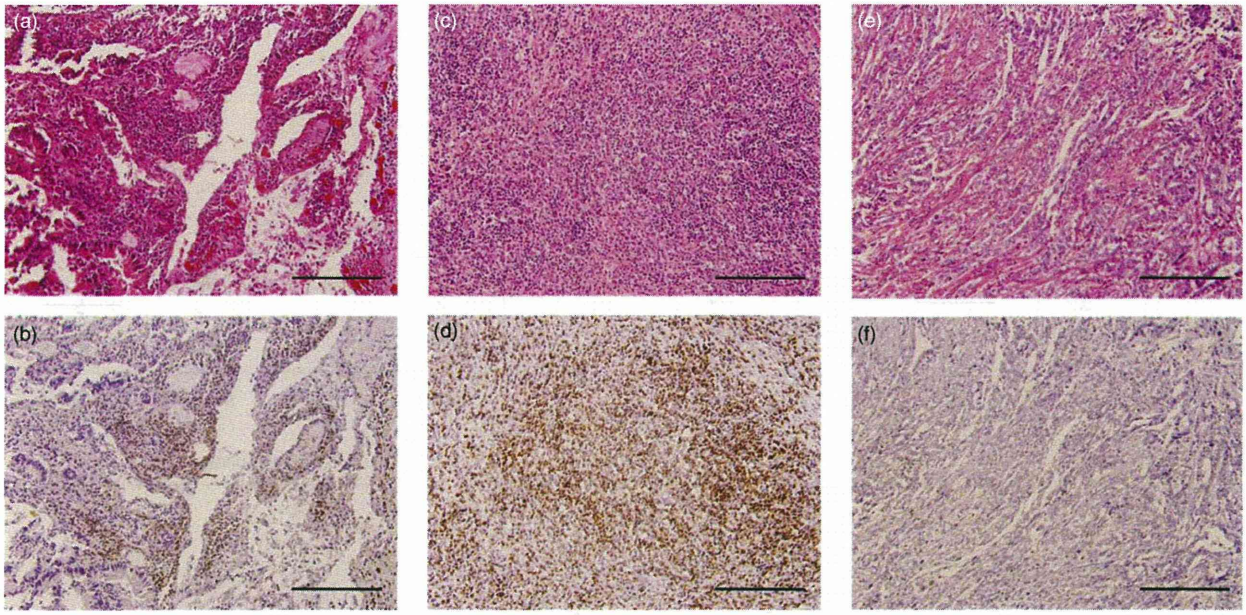

Figure 1 Representative immunohistochemical staining for CD3+ tumor-infiltrating lymphocytes (TILs) in gastric adenoma and cancer. Density of CD3+ TILs in gastric adenoma specimen (a, b). High density of CD3+ TILs in gastric cancer specimen (c, d). Low density of CD3+ TILs in gastric cancer specimen (e, f). Hematoxylin-eosin staining (a, c, e). Immunohistochemistry for CD3 (b, d, f). Scale bars indicate 200 μm (original magnification ×200).

Results

Density of CD3+ TILs in gastric cancer and adenoma. Based on immunohistochemical analysis, we assessed the density of CD3+ TILs in 120 and 27 PEAT specimens from patients with gastric cancer and adenoma, respectively (Fig. 1).

The numbers of CD3+ TILs ranged from 7 to 276 and from 181 to 598 in the gastric cancer and gastric adenoma specimens, respectively (Fig. 2). The mean number of CD3+ TILs (± SD) in patients with gastric cancer and adenoma was 87.5 ± 59.8 and 379.6 ± 128.1, respectively (Fig. 2). Consequently, significantly more CD3+ TILs were found in specimens from patients with gastric adenoma than with gastric cancer ($P < 0.0001$).

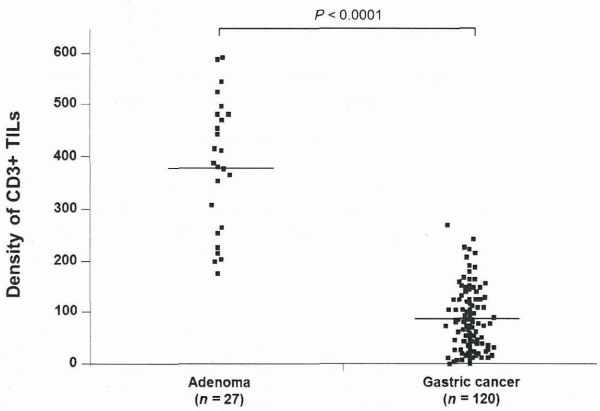

Figure 2 Immunohistochemical analysis of density of CD3+ tumor-infiltrating lymphocytes (TILs) in specimens from patients with gastric adenoma and cancer. Horizontal bars, mean numbers of CD3+ TILs.

Density of CD3+ TILs and clinicopathological factors. To determine its clinical significance during gastric cancer progression, we investigated whether CD3+ TIL density correlated with known clinicopathological prognostic factors for gastric cancer excluding lymph node status.

The numbers of CD3+ TILs did not correlate with sex, age, and histological type ($P = 0.804$, $P = 0.690$, and $P = 0.115$, respectively). We found a mean of 101.3 ± 42.0, 61.8 ± 48.7, 84.7 ± 72.9, and 77.1 ± 64.4 CD3+ TILs (± SD) in 44 pT1 tumors, 5 pT2 tumors, 34 pT3 tumors, and 37 pT4 tumors, respectively (Fig. 3a). The numbers of CD3+ TILs inversely correlated with depth of tumor invasion ($P = 0.022$). The mean (± SD) numbers of CD3+ TILs in 98 and 22 tumors without and with distant metastasis were 93.8 ± 61.3 and 59.5 ± 43.8, respectively. Significantly fewer CD3+ TILs were found in patients with, than without distant metastasis ($P = 0.015$). The mean numbers (± SD) of CD3+ TILs in 46, 16, 36, and 22 stages I, II, III, and IV cancers were 98.7 ± 42.8, 111.8 ± 86.8, 79.4 ± 66.6, and 59.5 ± 43.8, respectively (Fig. 3b). Stage-related differences in the numbers of CD3+ TILs were determined significant ($P = 0.011$). Similarly, the numbers of CD3+ TILs inversely correlated with the presence of lymphatic and venous invasion ($P = 0.002$ and $P = 0.0008$, respectively) (Fig. 3c,d).

Density of CD3+ TILs as a predictor of lymph node status. All patients were classified according to the criteria for the TNM classification of UICC (N0 *vs* N1 *vs* N2 *vs* N3) to assess

© 2014 Journal of Gastroenterology and Hepatology Foundation and Wiley Publishing Asia Pty Ltd

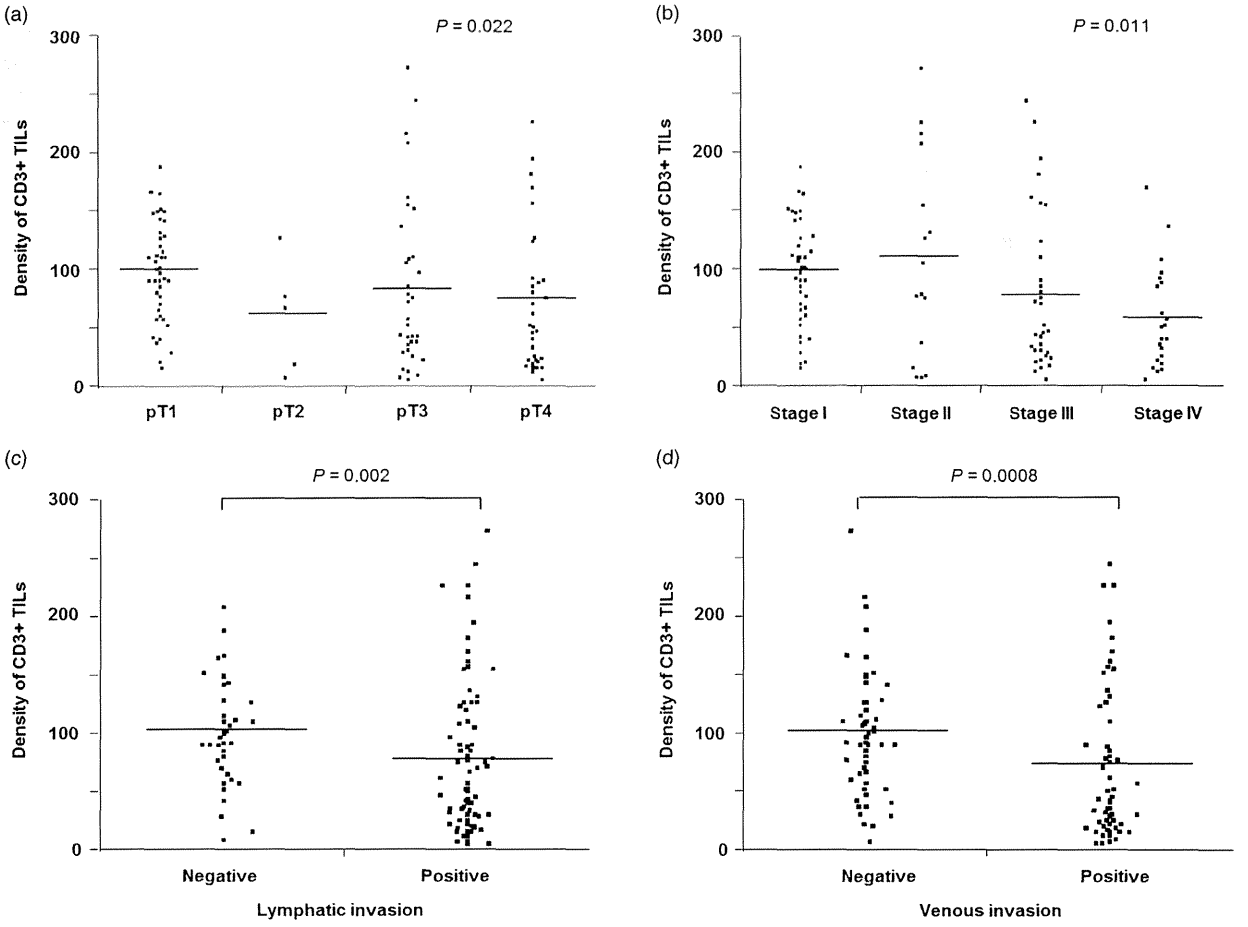

Figure 3 Correlation between density of CD3+ tumor-infiltrating lymphocytes (TILs) and clinicopathological factors in patients with gastric cancer. Numbers of CD3+ TILs significantly correlate with depth of tumor invasion (a), stage (b), lymphatic invasion (c), and venous invasion (d) ($P = 0.022$, $P = 0.011$, $P = 0.002$, and $P = 0.0008$, respectively). Horizontal bars indicate the mean number of CD3+ TILs.

the relationship between the density of CD3+ TILs and lymph node status. The density of CD3+ TILs (continuous variable) was significantly associated with increasing burden of lymph node status ($P = 0.0047$) (Fig. 4a).

According to the presence or absence of lymph node metastasis (N0 *vs* ≥ N1), patients with ≥ N1 had significantly less CD3+ TILs than those with N0 cancer ($P = 0.0004$) (Fig. 4b).

The predictive value of CD3+ TIL density for discriminating patients with and without lymph node metastasis was determined using the AUC of ROC curves. The AUC cut-off for the ability of CD3+ TIL density to discriminate patients with lymph node metastasis was 0.69 (Fig. 4c). The sensitivity and specificity for the density of CD3+ TILs were 0.73 and 0.65, respectively.

Density of CD3+ TILs and prognosis. We statistically evaluated the relationship between the density of CD3+ TILs and disease outcomes in 60 patients with more ($n = 60$) or less ($n = 60$) CD3+ TILs than the median.

The 5-year survival rates were significantly poorer for patients with less, than more CD3+ TILs (50.8% *vs* 84.2%, respectively; $P = 0.004$) (Fig. 5). Univariate analysis revealed histological type, depth of tumor invasion, lymph node metastasis, lymphatic invasion, venous invasion, and the density of CD3+ TILs as prognostic factors (all $P < 0.01$) (Table 2). Multivariate analysis selected the density of CD3+ TILs alone as an independent prognostic factor ($P = 0.034$) (Table 2).

Discussion

We investigated the density of CD3+ TILs in gastric cancer tumor foci and adenoma using immunohistochemical analysis. We also counted CD3+ TILs at each stage of gastric cancer and determined nodal status to determine changes in T-cell-mediated immune responses during tumor progression. To our knowledge, CD3+ TILs have not been quantified at each stage of gastric cancer and compared with nodal status.

© 2014 Journal of Gastroenterology and Hepatology Foundation and Wiley Publishing Asia Pty Ltd

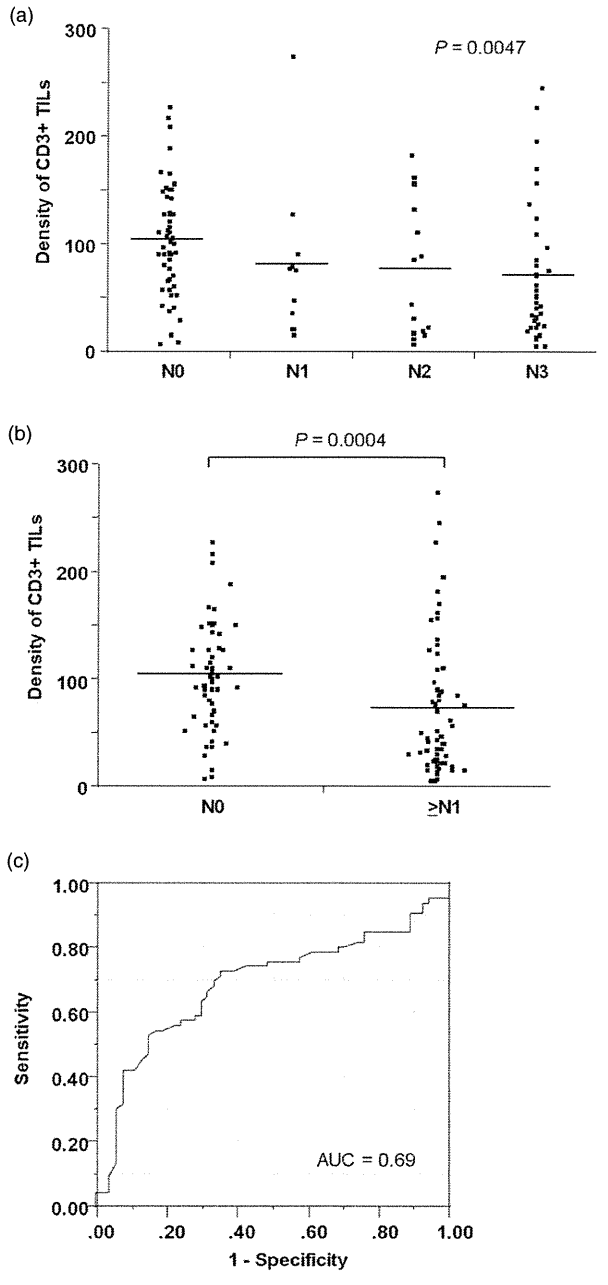

Figure 4 Correlation between density of CD3+ tumor-infiltrating lymphocytes (TILs) and lymph node status in patients with gastric cancer. (a) Relationship between CD3+ TIL density and increasing burden of lymph node status is significant ($P = 0.0047$). (b) Patients with ≥ N1 cancer had significantly fewer CD3+ TILs than patients with N0 cancer ($P = 0.0004$). (c) Receiver operating characteristic curve for discriminating patients with and without lymph node metastasis based on density of CD3+ tumor-infiltrating lymphocytes. Area under curve cut-off for discriminating presence of absence of lymph node metastasis was 0.69.

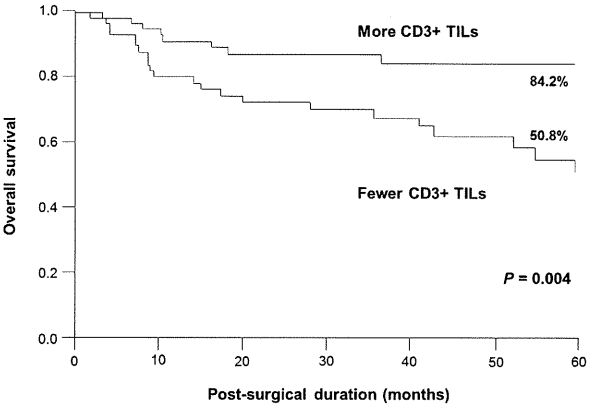

Figure 5 Kaplan–Meier survival curves for gastric cancer patients based on density of CD3+ tumor-infiltrating lymphocytes (TILs). Five-year survival rates are significantly poorer in patients with fewer CD3+ TILs ($P = 0.004$).

We initially compared the density of CD3+ TILs between gastric cancer and adenoma to assess differences in their immune environments. We found that patients with gastric adenoma had significantly more CD3+ TILs than those with gastric cancer ($P < 0.0001$). This finding indicated that CD3+ TIL-mediated activity in patients with gastric cancer is suppressed compared with that in patients with noncancerous disease. Furthermore, the numbers of CD3+ TILs determined as a continuous variable inversely correlated with established clinicopathological factors for tumor progression, namely, depth of tumor invasion, distant metastasis, and UICC stage ($P = 0.022$, $P = 0.015$, and $P = 0.011$, respectively). Lee *et al.* similarly demonstrated an inverse correlation between the numbers of CD3+ TILs and UICC stage in patients with gastric cancer, although the density of CD3+ TILs was not assessed as a continuous variable.[11] Laghi *et al.* reported that a higher density of CD3+ TILs significantly correlates with a lower risk of metachronous distant-organ metastasis in patients with colorectal cancer.[13] These results support the notion that tumor cells confer an advantage upon tumor progression by suppressing T-cell-mediated antitumor immunity.

The present study focused on the clinical applicability of CD3+ TIL density to predicting lymph node status. The TNM classification of the UICC categorizes lymph node status in gastric cancer as N0, N1, N2, and N3 based on the number of metastatic lymph nodes.[17] Lymph node status closely correlates with disease outcome in patients with gastric cancer. Consequently, the assessment of lymph node status is extremely important as a strategic issue for determining the indication of adjuvant or neoadjuvant chemotherapy in patients with advanced gastric cancer.[21,22] The present study indentified a close relationship between the density of CD3+ TILs and lymph node status, indicating that evaluating CD3+ TILs density in preoperative biopsy specimens might be useful as a predictor of lymph node status and as an indication for neoadjuvant chemotherapy in patients with advanced gastric cancer. On the other hand, patients with early gastric cancer are often treated by endoscopic resection such as endoscopic mucosal resection and endoscopic submucosal dissection.[23] However, a risk

© 2014 Journal of Gastroenterology and Hepatology Foundation and Wiley Publishing Asia Pty Ltd

Table 2 Univariate and multivariate analyses of survival in patients with gastric cancer

Independent factor	Univariate analysis			Multivariate analysis		
	Hazard ratio	95% CI	*P*	Hazard ratio	95% CI	*P*
Histological type						
Diff/Undiff	1.86	1.20–3.21	< 0.01	1.50	0.95–2.61	0.086
Depth of tumor invasion						
pT1–T2/pT3–T4	3.25	1.78–8.10	< 0.01	2.02	0.91–5.68	0.088
Lymph node metastasis						
N0/N1–N3	2.48	1.55–4.56	< 0.01	1.66	0.72–7.13	0.276
Lymphatic invasion						
Negative/positive	2.31	1.37–4.72	< 0.01	0.77	0.17–2.24	0.653
Venous invasion						
Negative/positive	2.10	1.39–3.45	< 0.01	1.09	0.67–1.95	0.750
Density of CD3+ TILs						
Lower/higher	0.57	0.37–0.83	< 0.01	0.65	0.42–0.97	0.034

Diff, differentiated; Undiff, undifferentiated.

of lymph node metastasis that persists after non-curative endoscopic resection is considered as an indication for additional surgery, according to the criteria of the Japanese Gastric Cancer Treatment Guidelines 2010 (ver. 3).[23–25] These guidelines define non-curative endoscopic resection based on several pathological findings of depth of tumor invasion, tumor size, histological type, involvement of horizontal and vertical margins, lymphovascular invasion, and ulcerative findings.[23] From the viewpoint of the close relationship between the density of CD3+ TILs and the presence or absence of lymph node metastasis determined herein, immunohistochemical analysis of CD3+ TIL density in endoscopic resected specimens might help to identify additional patients at high risk of lymph node metastasis after endoscopic resection.

Previous studies have demonstrated the predictive value of CD3+ TIL density for disease outcomes in various malignancies.[11–14] Lee *et al.* found that CD3+ TILs are significantly associated with better disease-free survival in patients with stage II colon cancer.[14] The 5-year survival rate in the present study was significantly poorer for patients with fewer CD3+ TILs ($P = 0.004$). Furthermore, the density of CD3+ TILs was an independent prognostic factor in the multivariate analysis ($P = 0.034$). Lee *et al.* similarly described significantly better survival among patients with a higher, than a lower density of CD3+ TILs in gastric cancer.[11] These results indicate that measuring CD3+ TIL density in surgically resected specimens might be helpful for considering the induction of adjuvant chemotherapy in postoperative patients with gastric cancer.

In this study, univariate analysis for assessing the prognostic value demonstrated that histological type, depth of tumor invasion, and lymph node metastasis were significantly related to postoperative survival ($P < 0.01$). However, these were not significant prognostic factors in multivariate analysis. This multivariate analysis extracted the density of CD3+ TILs alone as an independent prognostic factor. These results suggest that the density of CD3+ TILs might affect the values of known prognostic factors such as histological type, depth of tumor invasion, and lymph node metastasis in multivariate analysis. Furthermore, there are two possible explanations for these results: (i) The follow-up period was short (median, 36 months). (ii) The sample size may be too small for the verification of significant differences. In particular, the small sample size indicates one of clinical limitations in this study. Consequently, future validation studies will be needed to strengthen our findings in patients with gastric cancer.

A novel immunotherapy-targeted T-cell-mediated immune response has recently been attempted in patients with various malignancies.[26] In particular, the B7 family has been focused as a promising target in antitumor immunotherapy.[26] Tumor cells express the B7 ligand family and this signaling pathway promotes tumor progression via the downregulation of the T-cell-mediated immune response.[26] Cytotoxic T lymphocyte antigen-4 (CTLA-4) is a receptor for the B7-1 and B7-2 members of the B7 family, and a novel immunotherapy that blocks CTLA-4 has generated reliable response rates in phase I/II clinical trials.[26] We previously reported that the expression of B7-H4 inversely correlates with the number of CD3+ TILs in patients with gastric cancer.[27] These findings support the notion that tumor cells have an immune evasion mechanism by suppressing CD3+ TILs in patients with gastric cancer. In the future, CD3+ TILs will play an important role as an immune indicator for assessing the clinical value of immunotherapy in gastric cancer.

In conclusion, we demonstrated that the density of CD3+ TILs decreases during tumor progression and it is an immunological predictor for lymph node metastasis and a disease outcome in patients with gastric cancer. Further studies of the immunological behavior of CD3+ TILs including their association with a proliferative activity of tumor cells will facilitate the efficient development of immunotherapeutics for treating patients with gastric cancer.

Acknowledgments

We thank Ms. M. Tokunaga for excellent technical assistance. This study was supported in part by grants-in-aid (No. 25461955) for scientific research from the Ministry of Education, Science, Sports, and Culture, Japan.

References

1 Park JM, Kim YH. Current approaches to gastric cancer in Korea. *Gastrointest. Cancer Res.* 2008; **2**: 137–44.

© 2014 Journal of Gastroenterology and Hepatology Foundation and Wiley Publishing Asia Pty Ltd